Rapid thaw-driven geomorphic change transforms fluvial, sedimentary, and biogeochemical environments in the Willow River, NT

by

Jaedyn Linda Jasa Smith

A thesis submitted in partial fulfillment of the requirements for the degree of

Master of Science

in

Ecology

Department of Biological Sciences
University of Alberta

Abstract

The effects of global climate change are acute in permafrost environments. In the western Canadian Arctic, permafrost degradation of ice-rich slopes is resulting in the development of thermokarst and other forms of mass wasting, which transports previously frozen materials into aquatic systems. Here I examine the thaw-driven rejuvenation of the post-glacial sedimentary and geochemical cascade in the Willow River catchment (NT, Canada), an upland, ice-marginal setting where mass wasting is transforming erosional and depositional environments in response to shifts in thermal and hydroclimatic regimes. This transformation is evidenced by the diversion of the main Willow River channel through a delta lake (Willow Lake), causing a near-complete infill with sediments. Remote sensing analyses indicate that thaw-driven mass wasting features have increased in number (3.8-fold), size (9.2-fold), and density (16.3-fold) in the Willow River catchment since 1986, with expansion occurring non-linearly during the study period. This non-linear intensification has increased slope-to-stream connectivity within the system, resulting in increased turbidity within lakes lying along the new outflow channel, but decreased turbidity in lakes that lie along the abandoned channel. Cores taken from the alluvial surface of Willow Lake and nearby floodplain settings indicate clear shifts in depositional materials following the river rerouting. A coarsening upwards sequence indicates the development of a prograding delta within Willow Lake. Compositionally, materials varied with depositional energy and indicate dynamic post-depositional change in the sediment. This study provides evidence that thaw-driven erosion and mobilization of permafrost preserved glacial deposits is transforming the Mackenzie Delta, with major impacts on

Arctic depositional environments and carbon sequestration, which have the potential to shift ecosystem function within aquatic systems and cascade across watershed scales.

Preface

This thesis is an original work by Jaedyn Smith and is divided into three distinct chapters. The first chapter is an introductory chapter that provides background information on the field of research and study region, outlines the project objectives, and provides study rational and significance. The second chapter is written in manuscript format and is intended for publication. The final chapter is a general conclusion that provides a summary and recommendations for future work. Supervisory authors were Drs. Suzanne Tank and Steve Kokelj with further support from Drs. Duane Froese and Jon Tunnicliffe.

Chapter 2

Smith, J. L. J., Tank, S. E., Kokelj, S. V., Froese, D., Tunnicliffe, J., Korosi, J. Rapid thaw-driven geomorphic change transforms fluvial, sedimentary, and biogeochemical environments in the Willow River, NT. In preparation for publication.

Acknowledgments

I would like to start off by extending my immense gratitude to my supervisor, Dr. Suzanne Tank, for her guidance, support, and breadth of knowledge. I can confidently say that without Suzanne, the experience of this degree, from starting remotely, to five months of field work, to navigating lab work and writing, and everything in between, would not have been the positive experience that has allowed me to grow as a scientist, a leader, and as a person. The support of my committee has been invaluable throughout my degree. I would like to extend a big thank you to Dr. Steve Kokelj, whose help during the field season and feedback throughout my degree has provided valuable insights and perspectives that have really allowed me to develop a project that I am proud of. Thank you to Dr. Duane Froese and the PACS lab, and in particular Joel Pumple, for the methodical support that I did not know I would need (including ensuring I did not get trapped in the freezer after hours of cleaning my cores), but am immensely grateful for. Finally, I'd like to thank Dr. Jon Tunnicliffe, the unofficial member of my committee, for attending all committee meetings and offering invaluable advice, even with the 20-hour time difference.

Fieldwork for this project took place in the Gwich'in settlement region. Thank you to the communities of Aklavik and Inuvik, for being welcoming even during a pandemic. I would like to thank all of those who offered field support, including Alejandro Alvarez, Alexandre Chiasson, Davey Edwards, Grace Hoskin, Ryan McLeod, Sonny MacDonald, Marina Taskovic, and Alice Wilson. I am grateful for financial support from the University of Alberta, the National Science and Engineering Research Council, UAlberta North, the Northern Scientific Training Program, and the Weston Family Foundation.

Thank you to my amazing support network, who have helped push me through this degree. A special thank you to Nora Alsafi, Hayley Drapeau, and Marina Taskovic for starting remotely with me, guiding me through countless moments of imposter syndrome, and making me laugh until I cry. And, of course, thank you to the rest of the Tank Lab for listening to me make bad jokes about my piles of dirt. Finally, I'd like to thank my amazing partner, Ben Wright, for being the first set of eyes to read my writing, for magically guiding me through every statistical issue I faced, and for reminding me to breathe and go outside.

Table of Contents

List of tables

List of figures

Chapter 1. General introduction

1.1 Changing Arctic environments

Arctic regions are particularly susceptible to changes in climate, with a projected increase in surface temperatures that is 40% greater than the global mean by the end of the 21st century (1.1–2.6 °C, RCP 4.5; Pachauri et al., 2014). Warming Arctic temperatures are linked to increasing precipitation, with Arctic regions predicted to experience a shift from snow to rain dominated precipitation (Bintanja & Andry, 2017; Bintanja & Selten, 2014). Within the western Canadian Arctic, temperatures have increased 1.5–2.5 °C since the 1950s (Overland et al., 2011), and extreme precipitation events account for 50–70% of total precipitation since the 1970s (Yu & Zhong, 2021). These changes are either greater than or equivalent to other Artic regions (Overland et al., 2011; Yu & Zhong, 2021). Perennially frozen ground, or permafrost, is particularly sensitive to these changes in climate, with increased surface temperatures and changing snow cover causing permafrost temperatures to increase, resulting in thaw (IPCC, 2014; Romanovsky et al., 2010). Thawing permafrost can result in significant geomorphic alteration of the landscape and can result in the mobilization of previously frozen materials into nearby aquatic systems, which can substantially alter the biogeochemical processing of impacted environments (Kokelj & Jorgenson, 2013; Vonk, Tank, Mann, et al., 2015). This transfer of materials can have implications at scales ranging from global (the carbon cycle) to local (within-stream ecological function) and can cascade across watershed scales (Kokelj et al., 2021).

1.2 Thaw-driven mass wasting

As ice-rich permafrost terrain undergoes thaw, it can lead to thaw-driven mass wasting (i.e., thermokarst). Thermokarst represents a broad diversity of processes, the consequences of which can vary depending on the nature of permafrost and the type of thermokarst processes affecting the landscape (Kokelj & Jorgenson, 2013; Segal et al., 2016; Tank et al., 2020). The development of thermokarst is influenced by several factors such as climate, topography, ice content, and glacial legacy (Kokelj, Lantz, et al., 2017; Kokelj & Jorgenson, 2013; Segal et al., 2016). The presence of massive ice and ice

sediments within permafrost terrains of the western Canadian Arctic (Lacelle et al., 2004) make this area particularly susceptible to thermokarst development. Within hillslope regions, thawing of ice-rich permafrost terrain manifests in the form of retrogressive thaw slumps, which are the dominant form of thaw-driven mass wasting within this region (Lacelle et al., 2015). Ongoing changes in climate are causing thermokarst to accelerate in both initiation rate and disturbance magnitude (Kokelj & Jorgenson, 2013; Segal et al., 2016), with extensive permafrost terrain within the western Canadian Arctic primed for climate-driven change (Kokelj, Lantz, et al., 2017). In high-relief environments, rainfall is particularly influential in thermokarst initiation. As precipitation within Arctic environments shifts from snow to rain dominated, thermokarst initiation is likely to increase while streamflow switches from a purely nival towards a pluvial regime (Beel et al., 2020, 2021).

1.3 Impacts to aquatic systems

Accelerated thaw-driven mass wasting is causing increasing amounts of terrestrial material to be transported to nearby aquatic environments (Lacelle et al., 2010, 2015), resulting in significant increases in sediment loads within impacted streams (Kokelj, Lantz, et al., 2017; Kokelj, Tunnicliffe, et al., 2017). This increase in slope-to-stream connectivity can cause shifts in geomorphology, such as switching from fluvial incision to a phase of floodplain aggradation, when the connection is prolonged (Kokelj et al., 2013, 2021). Increased sediment mobilization can additionally alter the physical and biogeochemical functioning of impacted aquatic systems, in the form of elevated suspended sediments and turbidity, and associated higher concentrations of major ions, nutrients, and carbon (Beel et al., 2020; Kokelj et al., 2005, 2021; Kokelj, Zajdlik, et al., 2009). These changes can disrupt the ecological functioning of fluvial and lacustrine environments by impacting primary productivity, species abundance and diversity, and food web dynamics, the effects of which can cascade across trophic levels and remain for decades after disturbance (Beel et al., 2020; Blaen et al., 2014; Chin et al., 2016; Kokelj, Zajdlik, et al., 2009; Murdoch et al., 2021; Schuur & Mack, 2018; Vonk, Tank, Bowden, et al., 2015; Vucic et al., 2020).

1.4 Study region and rationale

The highlands of the Peel Plateau-Richardson Mountains region are characterized as having the largest relative area of thermokarst disturbance within the continuous permafrost zone of the western Canadian Arctic (Segal et al., 2016), and as being one of the most highly impacted landslide environments (Kokelj, Tunnicliffe, et al., 2017). Within this region, the Willow River catchment, located near Aklavik, NT, has been particularly subject to thermokarst disturbance, with thaw-driven mass wasting densities reaching greater than two-fold that of nearby catchments (Lacelle et al., 2015). This intensity has caused an estimated 40% of the stream network to be impacted by thermokarst, with an estimated 1.2 x 10^7 m^3 of materials displaced (Kokelj et al., 2021).

The materials exposed by permafrost thaw within this area are characterized by three distinct layers. At depth, tills deposited during the recession of the Laurentide Ice Sheet (LIS) have remained emplaced in permafrost and are largely unmodified, enabling sediments that are ice- and mineral-rich (A. Dyke & Evans, 2003; A. S. Dyke et al., 2002; Lacelle et al., 2004). Warmer temperatures during the early Holocene enabled active layers to deepen and undergo soil development, increased thaw-driven mass wasting, and enhanced talik development (Burn, 1997). Subsequent cooling promoted permafrost aggradation and preservation of these modified sediments in present-day permafrost. At the surface, the present-day active layer has undergone soil development, with accompanying incorporation of organic matter, and weathering of the mineral substrate (Zolkos & Tank, 2020). Each of these stratigraphic layers have different physical, geochemical, and organic carbon properties, which can impact aquatic systems differently when mobilized (Droppo et al., 2022; Lattaud et al., 2021; Shakil et al., 2020).

Notably, the Willow River drains directly into the Mackenzie Delta, a depositional environment that has been aggrading through the Holocene (Burn & Kokelj, 2009; Carson et al., 1999). This transition from fluvially-incised and thermokarst-affected uplands to a down-channel depositional environment has enabled a natural archive, whereby cumulative upstream thaw-driven geomorphic activity is captured in downstream settings. An example of this is the rerouting of the Willow River main stem in 2007, which occurred following enhanced sediment mobilization, as a result of upstream thermokarst and

transport downstream within the fluvial network. The main Willow River channel now discharges directly into Willow Lake, a large deltaic lake located along the edge of the Mackenzie River floodplain (Kokelj et al., 2021). High sediment loads within the river have caused the lake to be almost completely infilled with sediment, creating an archive of cumulative upstream impacts. These characteristics of the Willow River catchment have created an opportunity for a holistic study of the thaw-driven sediment cascade from mobilization, to transport, to deposition. By investigating the connections between these different environments, we are better able to link fluvial, sedimentary, and biogeochemical consequences in response to climate-driven permafrost degradation.

1.5 Research goals and objectives

This project focuses on understanding how the composition of fluvially-transported and deposited materials has changed as thaw-driven geomorphic activity has accelerated over the past several decades. Specifically, this study aims to assess the temporal impact of accelerated thaw-driven mass wasting on watershed geomorphology and how this has altered sediment mobilization, transport, and deposition within the Willow River catchment. The objectives of this project are threefold: First, to quantify the increase in thaw-driven mass-wasting features within the Willow River catchment since 1986. Second, to assess the impact of accelerated thaw-driven mass wasting on sediment delivery and transport within the aquatic network. Finally, to assess the degree to which materials derived from thaw-driven mass-wasting features are being deposited and modified in downstream environments. These objectives were accomplished by: (1) constructing a multi-decadal time series of thaw-driven mass-wasting features using remote sensing methods; (2) analyzing the connectivity between thawing slopes and stream channels and assessing historic changes in lake turbidity within the catchment; and (3) using a series of cores to create a temporal profile of the physical and biogeochemical properties of the sediment recently deposited within various aquatic and terrestrial environments that are connected to Willow River. These profiles were compared to a variety of upstream parent materials, as well as older constituents at depth.

1.6 Significance

To understand the connections between, and implications of, fluvial, sedimentary, and biogeochemical cascades in response to thaw-driven permafrost degradation, it is essential to investigate these environments holistically. The Willow River catchment has become highly disturbed, with profound geomorphic change driven almost entirely by recent shifts in thermal and hydroclimatic regimes. The rerouting of the lower channel outlet into a large lake (Willow Lake) at the edge of the Mackenzie Delta has created an unprecedented opportunity to study the composition of the recent sediment yield from the Willow River system. Comparing the materials found in the depositional area with key parent materials from eroding thermokarst features and stream banks will help elucidate their provenance and provide insight into how these modified materials cascade downstream. As thermokarst features increase in size, the nature of eroded materials changes because a greater proportion of mobilized sediments are derived from depth (Kokelj et al., 2021). This results in materials of increasingly divergent composition being transported by streams and rivers. It is therefore essential to characterize active layer, near surface permafrost, and sediments located deep within headwalls, and track their movement through fluvial systems.

The results of this research will also be of direct interest to nearby communities by providing valuable information on the historic and current effects of permafrost thaw on aquatic systems. This will supply community members and decision makers with information on how thermokarst-derived materials are impacting the nature of water resources in this region, as well as how permafrost thaw is impacting the landscape. The results of this project will help communities better understand and prepare for landscape disturbances that may impact community function, as well as inform decision makers when developing policies to combat and adapt to future changes in climate.

Chapter 2. Rapid thaw-driven geomorphic change transforms fluvial, sedimentary, and biogeochemical environments in the Willow River, NT

2.1 Introduction

Arctic regions are predicted to continue warming more rapidly than the global average, with a 40% greater increase in northern temperatures by the end of the 21st century(IPCC, 2014). This warming is expected to be accompanied by an intensification of the hydrologic cycle, following an increase in freshwater flux between the Arctic's atmosphere, land, and ocean domains (Bintanja & Andry, 2017; Rawlins et al., 2010). While warming and wetting have been pronounced throughout the pan-Arctic domain, the western Canadian Arctic has experienced changes in climate that are either greater than or equivalent to other Arctic regions (GISTEMP Team, 2022; Lenssen et al., 2019). Associated with this warming, the temperature of permafrost (perennially frozen ground) has increased due to increases in surface air temperature and declines in spring snow cover (IPCC, 2014; Romanovsky et al., 2010; Smith et al., 2005). The permafrost thaw that results from this warming can significantly alter the landscape, the effects of which depend on several environmental factors (Kokelj & Jorgenson, 2013; Tank et al., 2020).

In hillslope landscapes, ice-rich permafrost thaw can result in the loss of landscape structural integrity, which can lead to the development of collapse features, referred to as thermokarst. Retrogressive thaw slumps, a particularly dynamic form of thermokarst, are polycyclic in nature (Kokelj, Lantz, et al., 2009; Kokelj & Jorgenson, 2013). Exposure and thaw of ice-rich materials can initiate landscape collapse, while slumping materials that cover and protect the headwall can result in landform stabilization (Lacelle et al., 2010; Lantuit & Pollard, 2008). These features can reach up to 40 ha in size and can displace up to 10^6 m^3 of sediment (Kokelj et al., 2015). The western Canadian Arctic is an ice-marginal environment that was briefly covered by the Laurentide Ice Sheet (LIS) for ~7000 years during the late Pleistocene (Lacelle et al., 2013). Glacial presence and subsequent retreat have conditioned this landscape by enabling the emplacement and preservation of massive ground ice within present-day permafrost, priming this environment for rapid geomorphic change that can result in the erosion, mobilization, and sedimentation of

periglacially reworked terrain (Ballantyne, 2002; Kokelj, Lantz, et al., 2017). This glacial conditioning, coupled with warming and wetting trends, has enabled a clear acceleration of thermokarst activity in the western Canadian Arctic, with some of the largest disturbance areas recorded within the Peel Plateau-Richardson Mountains region (Kokelj et al., 2021; Kokelj & Jorgenson, 2013; Segal et al., 2016).

Accelerated thermokarst activity is tied to increasing connectivity between terrestrial and aquatic environments, which can result in large volumes of permafrost-derived materials being delivered to nearby streams, rivers, and lakes (Beel et al., 2021; Kokelj et al., 2021). Increased sediment flux within thermokarst-impacted streams can substantially alter fluvial geomorphology by shifting from fluvial incision to a phase of floodplain aggradation, with high sediment loads creating stream channel blockages (Kokelj et al., 2013, 2015). In addition, the delivery of novel biogeochemical constituents (e.g., organic carbon, nutrients) can alter primary productivity, species abundance and diversity, and food web dynamics in affected aquatic environments (Blaen et al., 2014; Chin et al., 2016; Mesquita et al., 2010; Vucic et al., 2020). Thus, this transfer of previously frozen terrestrial materials to aquatic systems can have wide-reaching impacts, and it is therefore critical to assess how these constituents vary across fluvial and sedimentary systems and the biogeochemical processes contained therein (Kokelj et al., 2021; Tank et al., 2020). This is particularly important in flowing water systems, where effects can cascade downstream and vary depending on considerations of physical processes and scale (Tank et al., 2020).

Slope-to-stream connectivity is facilitated by the development of debris tongues, where the accumulated sediments along the base of the retrogressive thaw slump are transported downslope (Kokelj & Jorgenson, 2013). Debris tongues mobilize materials that would otherwise accumulate in the scar area of thaw-driven mass-wasting features, transferring sediments into nearby aquatic systems that can be transported over long ranges and can result in downstream depositional blockades (Droppo et al., 2022; Kokelj et al., 2015). Thaw-driven changes in the physical and geochemical signatures of impacted aquatic systems can be expected to be observed for decades to centuries after initial disturbance (Beel et al., 2020; Kokelj et al., 2005; Shakil et al., 2020). Downstream

alluvial deposits capture materials mobilized and transported due to permafrost degradation, providing a natural archive of historic changes occurring upstream, and providing insight into the degree of slope-to-stream connectivity within the system (Mather et al., 2017). Materials trapped within alluvial deposits can be re-mobilized, indicating that these depositional environments can serve as a repository for future sediment delivery to downstream systems. Alluvial deposits can undergo transitions from subaqueous to subaerial, which drives dynamic post-depositional processes, such as soil development and terrestrialization (Shields et al., 2019). Investigating these changes, which can be expected to include the progression of weathering reactions and organic matter accumulation on and within alluvial deposits, will help to determine the effect of sediment mobilization on biogeochemical processes and downstream ecological function.

Here, we explore the effects of thaw-driven mass wasting across the land-water system within the Willow River catchment of the western Canadian Arctic. The Willow River, located near Aklavik, NT, is undergoing substantial thaw-driven geomorphic change, with an estimated 40% of the stream network affected by mass-wasting features. This ongoing landscape evolution has rerouted the Willow River main stem, causing it to flow through a large deltaic lake (Willow Lake) along the eastern margin of the catchment (Kokelj et al., 2021). Subsequent deposition of sediment within Willow Lake has created a unique opportunity to assess the biogeochemical, fluvial, and sedimentary impacts of thaw-driven mass wasting occurring upstream. Here we: (1) quantify the increase in thaw-driven mass-wasting features within the Willow River catchment since 1986; (2) assess the physical effects of thaw-driven geomorphic change on impacted fluvial and lacustrine environments; and (3) assess the change in physical and biogeochemical properties of materials deposited downstream with accelerated thaw-driven mass wasting. This was achieved by: (1) creating a multi-decadal time series of thaw-driven mass-wasting features using remote sensing methods; (2) analyzing the connectivity between thawing slopes and stream channels, and assessing turbidity trends within lakes of the Willow River catchment; and (3) creating a temporal profile of the physical and biogeochemical properties of sediment in depositional systems connected to the Willow River, and comparing these materials to upstream parent materials and older constituents deposited at depth.

2.2 Methods

2.2.1 Study area

The Willow River is an eastward flowing stream that drains the western margins of the Richardson Mountains, near Aklavik, NT. Its 800 km^2 catchment, with an elevation range to 1540 m asl, is underlain by continuous permafrost, with ~70% of the catchment lying within the glacial limit of the LIS, ~7% of the catchment lying within the lake-rich Mackenzie Delta floodplain, and the remaining ~30% consisting of colluvial slopes and exposed bedrock of the Richardson Mountains (Figure 2.1; Kokelj et al., 2017, 2021; Lacelle et al., 2010). The LIS advanced westward to the eastern slopes of the Richardson Mountains during the late Pleistocene, reaching its maximum extent ca. 18, 000 to 15, 000 calendar years before present (cal. ybp; Lacelle et al., 2013). This dynamic ice-marginal setting resulted in the emplacement of glacial tills hosting large volumes of relict ice in the form of preserved basal glacier ice and segregated ice (A. Dyke & Evans, 2003; A. S. Dyke et al., 2002; Lacelle et al., 2004). During the early Holocene (ca. 9, 000 cal. ybp), climate warming increased active layer thicknesses, thaw-driven mass wasting, and talik development, which enabled soil development via weathering of tills and incorporation of organic material into the soil profile (Burn, 1997; Zolkos & Tank, 2020). Climate cooling promoted aggradation of permafrost and the preservation of a thaw unconformity within the stratigraphic record (Burn, 1997). As a result, the materials exposed by thaw slumps within the Willow River catchment are characterized by three general layers: the seasonally thawed active layer, the previously thawed diamicton which underwent past soil development, and the ice-rich permafrost preserved Pleistocene tills at depth (Burn, 1997; Lacelle et al., 2004; Malone et al., 2013).

Modern-day reanalysis climate data for the Aklavik region has a mean annual air temperature (1961–1990) of -9.1 ºC, with a maximum temperature in July (13.6 ºC) and a minimum in January (-28.1 ºC, Mahony et al., 2022; Wang et al., 2016). Mean annual precipitation is 211 mm, with rainfall contributing approximately half of this value (102 mm). These values are comparable to long-term climate normals measured at the Inuvik station, located 75 km east of the study area, which has a mean annual air temperature (1961–1990) of -9.5 ºC and a mean annual precipitation value of 257.4 mm (Environment

Canada, 2022). Past analyses indicate that mean annual air temperature in the western Canadian Arctic has increased more than 2.5 ºC since the 1970s, with a major increase in precipitation occurring ~2010, based on Fort McPherson precipitation records, marking this region as one of rapid change (Burn & Kokelj, 2009; Kokelj et al., 2015).

It is estimated that about 40% of stream segments in the Willow River catchment are affected by various forms of thaw-driven mass wasting, most commonly in the form of thaw-slumping, but also including shallow slides, gullying, and a few deep-seated bedrock-controlled failures (Kokelj et al., 2021). The majority of the Willow River catchment is not lake rich, however several of the small upland lakes and ponds within the catchment are now also impacted by thaw-driven mass wasting. This geomorphic change is driven almost entirely by recent shifts in thermal and hydroclimatic regimes (Burn & Kokelj, 2009; Kokelj et al., 2015, 2021; Lacelle et al., 2004). This major increase in sediment transfer has modified drainage networks by increasing sediment storage in stream valleys in the form of debris tongues (Kokelj et al., 2021). Rapidly increasing stream sediment flux has caused the main Willow River outflow channel in the lake-rich Mackenzie Delta to reroute and drain directly into Willow Lake (Figure 2.1). This has produced an abandoned channel of ~40 km in length, which has left dozens of lakes and ponds without direct connection to the main Willow River channel but has increased connectivity to others along the low-gradient section of the catchment. Over the past decade, this rerouting has resulted in the near complete infill of Willow Lake, a 3.4 km^2 waterbody located within the low-gradient Mackenzie Delta. It is these geomorphic characteristics, paired with the glacial legacy and climate in this area, that make the Willow River catchment an ideal study region for the holistic analysis of thaw-driven erosion, sediment and geochemical transport, and deposition.

2.2.2 Geospatial analysis

The variation in thaw-sensitivity and distinct geomorphic environments within the rapidly changing Willow River catchment has created a unique opportunity to assess the cumulative impacts of thaw-driven mass wasting on downstream fluvial and depositional environments. Changes in thaw-driven geomorphic activity over the past several decades, and the historic and current impacts to downstream fluvial and lacustrine

environments were assessed using a variety remote sensing techniques. Remote sensing analyses were conducted in ArcMap Desktop Version 10.7.1.

2.2.2.1 Catchment delineation

The mapping extent for all work was confined to the Willow River catchment and surrounding areas. The catchment was delineated using digital elevation model (DEM) data obtained from USGS Earth Explorer. The catchment was digitized using a series of Spatial Analyst Hydrology tools in ArcMap Desktop including the tools Fill, Flow Direction, and Basin. The selected basins of interest were converted to polygons using the Raster to Polygon Conversion tool. The catchment was confirmed using the National Hydrology Network 10MC002 Shapefile package. The Willow River was digitized, and the Strahler stream order was determined using the Spatial Analyst Hydrology tools in ArcMap Desktop Flow Accumulation and Stream Order. River digitization was performed on the delineated catchment described above and confirmed using the National Hydrology Network 10MC002 Shapefile package.

2.2.2.2 Digitization of thaw-driven mass-wasting features

To determine the timing and pattern of increasing thaw-driven mass wasting and slope-to-stream connectivity, Landsat images (30-m resolution) were obtained from USGS Earth Explorer. A total of eight years were selected for analysis: 1986, 1992, 1996, 2001, 2007, 2011, 2017, and 2021. This frequency of analysis was selected to obtain a moderate to high temporal resolution of thaw-driven mass wasting evolution within the Willow River catchment. A combination of Landsat 4-5 TM, Landsat 7 ETM, and Landsat 8 OLI Collection 2 Level 1 products were used depending on the year of digitization. To reduce seasonal variation across years, all obtained images were from July 7–28. Images were selected to have a cloud cover below 15%. A combination of true colour and false colour images were used to identify and digitize all thaw-driven mass-wasting features within the Willow River catchment, permitting that they were active during at least one of the selected years (exposed sediment, unvegetated). While this analysis primarily focused on the identification of retrogressive thaw slumps, likely other mass-wasting features such as shallow and deeper-seated bedrock-controlled slides were included in our assessment.

All digitized landslides were split into scar zone and debris tongue components where downslope material transport was sufficient to form a debris tongue. The demarcation between the scar zone and debris tongue was defined as the first point of narrowed channelization within the feature (supporting information Figure A1). Features were also classified based on their connectivity to the stream network and/or adjacent water bodies. Mass-wasting features that had no identifiable connection to the aquatic network were classified with a connectivity of 0. Features that only had a scar zone, or had a scar zone and debris tongue, and were clearly in contact with the stream channel and/or water body, were classified with a connectivity of 1. Features that had a scar zone and debris tongue within the stream channel or lake were classified with a connectivity of 2 (supporting information Figure A2). Area (m^2) was calculated for all digitized features.

2.2.2.3 Grid cell visualization

Once the digitization of mass-wasting features was complete, the density distribution of features was visualized using the Fishnet tool in ArcMap Desktop, with 500 by 500 m cell sizes. For each unique cell, total feature area (cumulative scar zone and debris tongue area) was calculated using the Tabulate Intersection tool and the Pivot Table tool in ArcMap Desktop. From there, the density (%) of features was calculated following Equation 1. Five size classes were created for visualization purposes, with equal counts of grid cells based on the distribution of density (%) across all features identified in all years digitized.

$$\text{Equation 1. Density (\%)} = \frac{\text{Total Feature Area (m}^2\text{)}}{\text{Cell Area (m}^2\text{)}} \times 100$$

2.2.2.4 Turbidity analysis for lakes

In order to assess the influence of increased thaw-driven mass wasting and channel rerouting of the lower Willow River on upland and Delta lakes, all lakes within the catchment were digitized and grouped into a series of geomorphic categories that reflect catchment location and source water characteristics (Table 2.1). “Upland” lakes are situated within glaciated portions of the Willow River catchment in hummocky moraine and colluvial deposits. These lakes are typically small, and many are directly affected by retrogressive thaw slumps. Lakes classified as “abandoned” are located within the

Mackenzie Delta component of the catchment and are situated along the abandoned Willow River channel (Figure 2.1). Similar to “abandoned” lakes, “rerouted” lakes are located within the Mackenzie Delta component of the catchment. However, these lakes lie along the new outflow channel from the Willow River, which travels through Willow Lake before flowing into the Peel Channel of the Mackenzie Delta. In addition to the direct connection between “rerouted” lakes and the Willow River, both “rerouted” and “abandoned” alluvial lakes are flooded by the Mackenzie Delta, with river-to-lake connectivity greatest during the annual spring flood (May–June; Marsh & Hey, 1989). A buffer zone between “abandoned” and “rerouted” lakes was implemented to ensure a clear demarcation between these two lake categories. A subset of four lakes within the “rerouted” zone, classified as “sampled” lakes, were independently analyzed to assess turbidity changes within waterbodies that have physical samples associated with them (see below). Finally, several lakes along the Husky Channel that fall outside of the Willow River catchment were digitized as reference lakes, (termed “Husky”, below). These waterbodies are located in an alluvial setting and are subject to inflows from the Mackenzie Delta. However, because they lie upstream of where the Willow River enters the Mackenzie Delta, they have not been impacted by changes affecting the Willow River catchment.

All water bodies within the Willow River catchment were digitized using a combination of Landsat 4-5 TM and Landsat 7 ETM Collection 2 Level 1 products. A total of eight years were selected for analysis. Most of the images used were the same as those selected for thaw-driven mass wasting feature identification (1986, 1996, 2001, 2007, 2011), with three exceptions based on cloud cover and geographic extent (1990, 2017, 2022). All images used were from July to capture active sediment flow from active thaw-driven mass-wasting features, while minimizing Deltaic inflows from the Peel Channel in spring and early summer. Only water bodies that consistently displayed open water conditions across all years and had surface waters that were less than 50% impacted by missing data (i.e., Landsat 7 ETM scan line errors) were digitized. Water bodies were digitized with a one-pixel buffer from lake edges to remove shoreline influence. Turbidity was calculated using the normalized difference turbidity index (NDTI) following Equation 2 (Bid & Siddique, 2019; Garg et al., 2020; Lacaux et al., 2007).

Reflectance values from band 2 (red) and band 3 (green) were extracted from the Landsat images, with mean reflectance of digitized water bodies calculated using the Zonal Statistics as Table tool in ArcMap Desktop. NDTI was calculated as a mean value over each water body digitized.

$$\text{Equation 2. NDTI} = \frac{\text{Red Band} - \text{Green Band}}{\text{Red Band} + \text{Green Band}}$$

2.2.3 Temporal trends in sediment sequestration in downstream depositional lakes

2.2.2.5 Sample collection

To investigate how changing geomorphic activity has affected the composition of sediments in depositional environments within the Willow River catchment, samples were collected from a variety of parent materials (Table 2.2) that might reasonably contribute to riverine sediment load, coupled with core samples from forested overbank alluvium, the alluvial surface within Willow Lake, and connected downstream lacustrine environments. Several helicopter-accessible thaw-driven mass-wasting features, were identified for sampling to capture varying degrees of landscape disturbance (headwall samples, Figure 2.1a). At these locations (H4, H8), lateral cores of permafrost headwall and bulk samples of scar zone sediments were collected either in spring 2021 under frozen conditions, or summer 2021 under thawed conditions. A landslide (H7) was sampled via the collection of colluvium in approximately the centre of the eroding feature. A series of river cut bank samples were additionally collected at sites upstream (CB2) and downstream (CB5, 8) of sampled permafrost headwalls and at a site at the inflow (CB9) to Willow Lake. Cut banks were sampled from the exposed eroding surface at a midpoint depth. Finally, a stream bed sample (SB10) collected at the outflow of Willow Lake was also included in the suite of parent materials due to the visible dual direction of flow at this site, which captures depositional sediments from both the Willow and Peel Rivers.

In the spring of 2021, a team of academic researchers and Gwich'in land users collected a series of sediment cores to assess the characteristics of lake bottom deposits in a series of small lakes reflecting a turbidity gradient connected to Willow Lake, alluvial

deposits of the prograding delta within Willow Lake, and overbank alluvium in forested environments (Figure 2.1). Three boreholes were drilled to depths of up to 3.5 m using a Cold Regions Research and Engineering Laboratory (CRREL) core barrel to obtain alluvial deposits that have accumulated within the prograding delta of Willow Lake. Borehole locations were selected to capture changes in depositional energy within the prograding delta, as well as capture variations in the nature of deposition through time. The most proximal core to the distributary channel (AC3) reflects a high energy environment along the most elevated active alluvial surface, while the most distal core (AC1) reflects decreasing depositional energy and the lowest elevation (Figure 2.1). Along this transect, core depths measured 358 cm (AC1), 123 cm (AC2), and 148 cm (AC3), such that the most distal core location also provided the greatest depth of record (and likely the deposits predate recent rerouting of the Willow River). A core was also collected from forested alluvial surfaces near a cut bank upstream of the river inflow to Willow Lake (TC1), which we hypothesize captures the transition from recent, high-energy flooding, to lower sedimentation rates at depth, prior to the rerouting of the Willow River. An additional core was collected from a forested alluvial surface along the shoreline of Willow Lake (TC2), distal to the Willow River inflow (infrequent, relatively low-energy flooding) to assess the characteristics of materials deposited during overbank flooding before and after rerouting of the Willow River. To assess the nature of lacustrine deposits beyond the large aggrading delta within Willow Lake and to examine recent changes in sedimentation with increasing sediment flux from the Willow River catchment, Uwitec Gravity Cores (90 mm diameter) were taken from a chain of three delta lakes connected to Willow Lake (LC1 – LC3). This lake chain receives inputs from the Peel Channel of the Mackenzie Delta by overbank flooding during spring (Marsh & Hey, 1989, 1994), and more recently, by the increased sediment flux from the Willow River as it has rerouted into Willow Lake due to intensification of thaw-driven mass wasting. Historically, this lake chain has also received inputs via the influx of backwater into Willow Lake with increases in Peel Channel or the pre-diversion Willow River water levels, and reflects a turbidity gradient.

Bulk sediment and CRREL core samples were transported to the University of Alberta in a frozen state (-20 °C) and stored frozen until processing. Unfrozen gravity core

samples were transported to the field laboratory to be sectioned in 0.5 cm intervals for the upper 10 cm of core, and in 1 cm intervals for the remaining core. Samples were frozen and later transported to York University and stored (-20 °C) until further processing.

2.2.2.6 Sample processing

Frozen CRREL cores were processed at the Permafrost Archives Science (PACS) Lab at the University of Alberta. Cores were cut in half vertically using a diamond blade table saw to expose the inner cross-section of the cores. One-half of each core was immediately archived. To remove surface debris and prepare core samples for imaging, the working halves of the cores were cleaned using metal razor blades. Following this, core sections were analyzed for magnetic susceptibility (SI e^{-5}) and density (g cm^{-3}) using a Geotek Standard Multi-Sensor Core Logger (MSCL-S) in 0.5 cm intervals. Ultra high-definition core images were also obtained using the Geotek MSCL-S. A combination of magnetic susceptibility, density, and high-definition images were used to identify facies within each core, which were used to dictate the sub-sectioning frequency (Supporting information, Figures A3–A8). The working halves of the cores were again halved using a table saw and cleaned with ceramic razor blades to remove metal contamination introduced from prior cleaning and cutting. Cores were cut into ~10 cm vertical sections, with some variations based on identified facies (Supporting information, Figures A4-A8). CRREL and gravity core sections, lateral cores (i.e., of parent material), and bulk sediment samples, were all freeze-dried and homogenized using a mortar and pestle. Modest pressure was applied when homogenizing the samples to preserve grain size fractions.

2.2.2.7 Sample analysis

To assess the bulk organic content of samples, Loss on Ignition (LOI) analysis was conducted on freeze-dried materials. Samples were weighed and combusted at 550°C for 4 hours to remove organic materials (Heiri et al., 2001; Dean, 1974). Following combustion, samples were allowed to cool at 60°C for 1 hour before recording the mass. The organic matter content (%) of samples was calculated using Equation 3. The remaining combusted material was then used to characterize the grain size distribution of each sample. Combusted samples were sieved to 1000 μm to avoid damage to the

sample dispersion unit by larger particles. Samples were treated with a 5% w/w solution of Sodium hexametaphosphate prior to laser diffraction analysis using the Malvern Mastersizer 3000 to prevent particle aggregation (D422-ASTM, 1972). All samples for grain size were analyzed in duplicate. Median grain size (μm) was identified in volume (%) for the analyzed fraction.

$$\text{Equation 3. } \% = \frac{[\text{Weight Freeze Dried Sample}] - [\text{Weight of Post 550 °C Ash}]}{[\text{Weight Freeze Dried Sample}]} \times 100\ \%$$

To assess nitrogen, organic carbon, and sulfur content, freeze-dried samples were further ground to a fine flour (<500 μm) and weighed to the thousandth milligram into tin (nitrogen, sulfur) or silver (organic carbon) capsules to prepare for encapsulation (described below). For the analysis of organic carbon, a heated acid-fumigation (37% trace metal grade HCl, 60°C) was performed for 72 h to remove inorganic carbon present in the samples (Harris et al., 2001; Ramnarine et al., 2011; Whiteside et al., 2011). Prior to the start of the fumigation, samples were wetted with a small amount (~50 μL) of dilute (1% trace metal grade HCl) acid (Ramnarine et al., 2011; Walthert et al., 2010) to aid the fumigation process. Following fumigation, samples were neutralized in a desiccator with NaOH pellets for 24 hours and then allowed to dry at 60°C for 16 hours before being encapsulated. Samples analyzed for total nitrogen and sulfur were encapsulated without fumigation in the original tin capsules, and samples analyzed for organic carbon were encapsulated with a tin sleeve surrounding and enclosing the original silver capsule. Samples were analyzed for organic carbon and nitrogen at the Stable Isotope Facility located at the University of California, Davis and for sulfur at the Jan Veizer Laboratory at the University of Ottawa. Although similar, methods at each facility vary slightly. Samples analyzed at the Stable Isotope Facility were combusted at 950 °C in a reactor with chromium oxide and silvered copper oxide. Following combustion, oxygen and nitrogen oxides were removed and CO_2 and N_2 were separated before the gas analyte was measured using one of six EA-IRMS systems. For samples analyzed at the Jan Veizer Laboratory, Tungsten (VI) oxide was included in the capsules prior to encapsulation as a catalyst, and samples were analyzed with the elementar Isotope Cube following flash combustion at 1800°C. Organic carbon, nitrogen, and sulfur content are expressed as percent values by mass analyzed. Organic carbon and nitrogen values

were used to calculate the molar ratio of carbon to nitrogen (C:N). This ratio is expressed as nitrogen to carbon (N:C) when plotted in direct comparison with other carbon parameters (Perdue & Koprivnjak, 2007).

To evaluate sediment accumulation rate and date of deposition, gravity core samples LC1, LC2, and LC3 were analyzed for radioisotopes ^{214}Bi, ^{137}Cs, ^{210}Pb, and ^{214}Pb using a gamma counter at the Paleoecological Environmental Assessment and Research Laboratory (PEARL) at Queen's University (Schelske et al., 1994).

Mineral identification was conducted via X-ray Diffraction (XRD). Freeze-dried samples were ground to a fine powder (<40 μm) using a mortar and pestle prior to analysis at the X-ray Diffraction Laboratory at the University of Alberta. Phase identification was conducted using a Rigaku Ultima IV X-Ray diffractometer. Sample diffraction patterns were matched against the XRD database available at the laboratory to provide presence-absence data with a detection limit ranging from 1–5 wt%.

Analysis of cation composition was conducted via inductively coupled plasma mass spectrometry (ICP-MS). To analyze samples for cation composition, 0.25 g of sample was weighed into Teflon vessels with 10 mL of trace metal grade nitric acid. Vessels were sealed and allowed to fumigate for 30 minutes. Following this, samples were microwave digested using a CEM MARS6 Microwave Digestion System for approximately one hour. The microwave digestion used a temperature ramp up to 200 °C over a 20-minute period, and then maintained that temperature for an additional 15 minutes (American Public Health Association et al., 1999). Digested samples were then decanted into 50 mL centrifuge tubes. The Teflon vessels were rinsed in triplicate with 18.2 MΩ (MilliQ) water, the product of which was added to respective centrifuge tubes. The centrifuge tubes were then filled to the 50 mL mark with 18.2 MΩ water. Samples were then stored chilled (4°C) until analysis at the CALA (Canadian Association for Laboratory Accreditation) accredited Biogeochemical Analytical Service Laboratory at the University of Alberta, where the samples were analyzed using an Agilent 7900 ICP-MS.

To assess radiocarbon (Δ^{14}C) content of organic carbon in sediment, samples were ground to a fine powder (<63 μm) using a mortar and pestle prior to being analyzed at the André E. Lalonde AMS Radiocarbon Laboratory at the University of Ottawa. Pre-

treatment of samples followed standard laboratory procedure, including calibrating samples based on geographical information provided, inspecting samples for signs of possible contamination, and acid washing (HCl, 1N, 80°C, 30 min) followed by an alkali rinse (NaOH, 0.2N, 80°C, 30 min) to remove inorganics (Crann et al., 2017; Murseli et al., 2019). Samples were analyzed using the Ionplus AG MICADAS (Mini Carbon Dating System) and processed using the data reduction software (Stuiver & Polach, 1977; Wacker et al., 2010).

2.2.4 Statistical analyses and data visualization

All statistical analyses were conducted in R version 4.2.0 (R Core Team, 2022) including frequently used packages *ggplot2*, *reshape*, and *stringr* (Wickham, 2007, 2016, 2019). A linear regression was conducted on reanalysis climate data to visualize trends in mean annual and mean summer temperature and precipitation. Using the R package *lme4* (Bates et al., 2015), linear mixed effects models were used to assess the influence of year on lake turbidity for each lake category. Models included year as a fixed effect and lake as a random effect. Breakpoints in linear turbidity trends among years for each lake category were calculated using the R package *segmented* (Muggeo, 2003, 2008). The packages *tidyverse* and *tidypaleo* were used to create stratigraphic diagrams for physical and biogeochemical properties (Dunnington et al., 2022; Wickham et al., 2019). To compare mineralogy (XRD) among samples, a non-metric multidimensional scaling (NMDS) was implemented using the package *ecodist* (Goslee & Urban, 2007). A principal component analysis (PCA) was used to compare cation composition among samples, using the R package *ggfortify* (Horikoshi & Tang, 2018; Tang et al., 2016).

2.3 Results

2.3.1 Rapid acceleration of thaw-driven mass wasting occurs in association with warming and wetting trends

Reanalysis climate data for the Aklavik region from 1986–2021 shows significant linear increases in mean annual temperature of ~0.06 ºC y^{-1} (Figure 2.2a) and mean annual precipitation of ~1.95 mm y^{-1} (Figure 2.2b). When looking at summer trends, mean

summer temperature is declining linearly at ~0.008 ºC y^{-1} (Figure 2.2c), and mean summer precipitation is increasing linearly at ~1.46 mm y^{-1} (Figure 2.2d).

These temperature and precipitation trends are reflected in the increase in size, abundance, and density of thaw-driven mass-wasting features within the catchment (Figure 2.3). The total area and number of identified features since 1986 reveal a greater than nine-fold increase in total disturbance area (9.16), and a nearly four-fold increase in the total number of identified features (3.75, Figure 2.3b). There was also a greater than six-fold enlargement of total debris tongue area (6.15) and a greater than 11-fold growth of total scar zone area over the same time period (11.61). GIS-enabled mapping indicates a seven-fold increase in the number of unique debris tongues since 1986, which corresponds to a greater than five-fold increase in features identified that connect directly to the aquatic network (connectivity level 2, 5.6-fold increase, Figure 2.3c). Level 0 and 1 connectivity features, which do not connect directly to the aquatic network, have also increased, but at a lower overall rate (3.4 and 2.9-fold, respectively).

A grid-cell analysis of thaw slump density revealed that thaw slump intensification concentrated within the eastern, glaciated portion of the catchment at elevations ranging from 40–660 m asl. While grid cells classified as having 10–70% feature density increased 16-fold from 1986–2021, there was a less than three-fold increase in prevalence of the three lowest density bins (0-4%).

2.3.2 Intensification of thaw-driven mass wasting results in increased lake turbidity

Increases in thaw-driven catchment erosion, and their cascading effects, have recently altered the configuration of downstream depositional environments. This warrants an investigation into the diversity of impacts on lake turbidity in different geomorphic settings throughout the catchment. Across the study period, upland slump affected, as well as rerouted, rerouted-sampled, and Husky Channel lakes in the Delta all show an increase in NDTI, with rerouted-sampled lakes and Husky lakes showing the strongest and weakest changes, respectively (Table 2.4). Delta lakes along the

abandoned channel are the only waterbodies that show a decline in NDTI across the 1986–2021 study period.

Upland lakes show a substantial positive trend in NDTI, with the narrowest confidence intervals of the analyzed lake types (Table 2.4, estimate = $1.4 \times 10^{-3} \pm 0.3 \times 10^{-3}$ 95% CI), and relatively minor within-year NDTI variation among lakes (interquartile range (IQR) = 0.103; IQR is expressed as the difference between the smallest lower quartile value and the largest upper quartile value across the study period; Figure 2.4a). In lakes adjacent to the recently rerouted channel, variability is consistently high among lakes across all years (Figure 2.4c, IQR = 0.183), with a clear NDTI increase since 1986 (Table 2.4, estimate = $1.3 \times 10^{-3} \pm 0.4 \times 10^{-3}$). The rerouted-sampled lakes in this study (comprised of Willow Lake and the three lakes from which gravity cores were obtained) showed an overall positive NDTI trend, but with confidence intervals that were the widest of all lake categories (Table 2.4, estimate = $1.9 \times 10^{-3} \pm 1.0 \times 10^{-3}$). Variation among lakes is also high across all years, typical of lakes sampled across a gradient of impact intensity (Figure 2.4d, IQR = 0.184). The lakes on the west side of Husky Channel show an increase in NDTI that is weakly positive with moderate confidence intervals (Table 2.4, estimate= $0.9 \times 10^{-3} \pm 0.4 \times 10^{-3}$), with the lowest variability among lakes (Figure 2.4e, IQR = 0.087). In contrast to the other lake categories, there was an overall weak negative NDTI trend observed within abandoned lakes since 1986, with relatively wide confidence intervals (Table 2.4, estimate = $-0.4 \times 10^{-3} \pm 0.6 \times 10^{-3}$), however this trend appears to be largely driven by a decline in turbidity after 2007 (Figure 2.4b), which was accompanied by a significant decrease in variability at this time (IQR shift from 0.198 to 0.052).

An investigation of NDTI trend break points throughout the analysis period reveals clear shifts in either trend directionality or trend magnitude for all lake categories. Although an overall positive trend was observed for upland lakes, there has been a recent shift from an increase in turbidity during 1986–2017 (Table 2.5, estimate = 1.9×10^{-3}), to a decline in turbidity since 2017 (estimate = -3.6×10^{-3}). The turbidity of rerouted lakes increased at a greater rate between 1986 and 1996 (Table 2.5, estimate = 2.9×10^{-3}) than during 1996–2022 (estimate = 0.9×10^{-3}). Three trend periods were identified for the rerouted sampled lakes, with an increase in turbidity observed between 1986 and 1996

(Table 2.5, estimate = 6.4 x10^{-3}), a decline in turbidity during 1996–2007 (estimate = -3.0 x 10^{-3}), and a notable increase in turbidity following the rerouting of the main stem in 2007 (estimate = 4.3 x 10^{-3}). Although an overall positive trend is observed in Husky channel lakes, there have been two periods of turbidity change observed since 1986, with a weakly negative trend in turbidity observed during 1986–2001 (Table 2.5, estimate = -0.3 x 10^{-3}) followed by a shift to increasing turbidity since 2001 (estimate = 1.6 x 10^{-3}). Three trend periods were observed for abandoned lakes, with a positive trend between 1986 and 2007 (Table 2.5, estimate = 3.0 x 10^{-3}), a strongly negative trend between 2007 and 2017 (estimate = -17.1 x 10^{-3}), and a recent shift back to increasing turbidity since 2017 (estimate = 7.1 x 10^{-3}). All lake categories analyzed showed a greater NDTI in 2022 than in 1986, with the greatest increase observed in rerouted and rerouted-sampled lakes.

2.3.3 Fluvial alteration is captured within depositional environments

2.3.3.1 Stratigraphic parameters

The alluvial and terrestrial cores were classified into six facies based on visual characteristics, density (g cm^{-3}) and magnetic susceptibility (SI e^{-5}; Table 2.3, Figure 2.5, Supporting Information Figure A3). Facies A–E were primarily identified in the cores taken from the alluvial surface of Willow Lake, with Facies A and B also identified within the forested alluvial plain (Figure 2.6). Facies F was found only in the cores taken from forested alluvial surfaces. Facies A is characterized by a combination of coarse and very fine-grained sediments (coarse sand to silt), high organic content (visually observed presence of plant debris), low density, and low magnetic susceptibility. This facies appears to represent historic alluvial surfaces that accumulate organic materials that settle as floodwaters recede, as well as the incorporation of surface vegetation that is buried by alluvial sedimentation. Facies B is comprised of typically coarser-grained materials (very fine sand to coarse sand), high density, and moderate magnetic susceptibility, which is typical of deposition in higher energy environments of a prograding delta. Facies C is dominated by medium-grained sediment (very fine sand), high density, high magnetic susceptibility, and hosts thin lenticular ice lenses characteristic of aggradational ice (Kokelj & Burn, 2005). Facies D is comprised of finer-grained sediment (silt) that is typically darker in colour and has a higher ice content (thin reticulate

cryostructure) when compared to Facies B and C. These characteristics are consistent with sediment deposited in a lower energy environment. Facies E has the finest-grained sediment and the highest ice content of all facies characterized, with thin lenticular and reticulate cryostructures hosted in fine silt. This facies is typically lighter in colour than Facies D, and is greyish in comparison with the brown colours observed in Facies B and C. Facies A through E are associated with the prograding delta depositional environment, which in cross-section shows the outward growth of the Willow Lake delta through time (Figure 2.6). In contrast to Facies A–E, Facies F is characterized predominantly by organic materials, low density, and low magnetic susceptibility. This facies appears to capture characteristics typical of a forest floor and serves as a reference facies for the infrequently flooded forested alluvial environments with low rates of sedimentation.

2.3.3.2 Parent materials

All parent materials sampled from the catchment have a medium to coarse grain size similar to that observed in Facies B and C (25–50 μm), except for sample CB2 (upland eroding landslide as cut bank; ~200 μm, Figure 2.7). Parent materials are consistent across samples in terms of percent organic content (%organics), organic carbon (%OC), and nitrogen (%N; ~5%, 2%, and 0.1%, respectively) with the exception of CB2, which has higher % organics and %OC (~10% and 4%, respectively), and H4-AL (near-surface active layer), which has higher % organics, %OC, and %N (~27%, 15%, and 0.75%, respectively). Barring the outlying samples, the range of values for %organics in parent materials is most similar to Facies D, %OC is most similar to Facies B, and %N is most similar to Facies B and C. Of the analyzed parameters, percent sulfur (%S) is more variable across parent materials, with a range of values from 0–1%, with CB2 as an outlier (2%). Similarly, the molar ratio of carbon to nitrogen (C:N) is variable across the sampled parent materials, with a range from 8–20, with CB2 again as an outlier for this parameter (~30). Both %S and C:N values for parent materials fall within ranges that align with at least one of the identified facies described above.

2.3.3.3 Prograding delta- Willow Lake cores

The upper 70 cm of the most distal and lowest elevation core from the aggrading Willow Lake delta (AC1) had physical and biogeochemical characteristics that are distinct

from greater depths in the core, and most closely align with the range in characteristics observed for AC2 and AC3 (Figure 2.8). With the exception of the surface 6 cm, the upper 70 cm of AC1 is characterized by relatively larger grain size and higher density and magnetic susceptibility, a low %OC, %N, %S, and %organics. C:N is relatively high in this section and decreases with depth. At 70cm, AC1 undergoes a clear shift from coarser-grained sediments that are lighter in colour (corresponding with Facies B and C), to darker, fine-grained sediment with modest, but slightly elevated, organic and ice content (70 – 270 cm, Facies D) at depth. The bottom of AC1 (270–360 cm) is composed of finer-grained sediment, high %organics and ice content, and relatively higher %N and %OC (Facies E). Below 70 cm depth, there is a decreasing trend in grain size, sulfur, and C:N, whereas there is a modest increasing trend in % organics, %OC, and %N with depth. Within this core, Facies E appears to be characteristic of materials deposited prior to the river reroute, Facies D appears typical of conditions associated with sediment deposition in a low energy environment, while Facies B and C display characteristics consistent with the most recent transition to a higher energy prograding delta surface.

The remaining two alluvial cores taken from Willow Lake are approximately half the length of AC1 and are from a higher elevation closer to the apex of the prograding delta. These cores (AC2, 3) capture the signatures of these depositional environments, with typically larger, more variable grain sizes, representing the high energy and dynamic nature of this depositional setting. The stratigraphic characteristics of the upper 70 cm of AC1 are reflected in the trends seen in AC2 and AC3, and most closely overlap with parent materials (Figure 2.7; Figure 2.8), however there are some notable differences that likely reflect the high energy nature of these more river-proximate depositional settings. In AC2, there are two organic-rich sections that align with Facies A (0–7 cm, 74–79 cm) which show high %OC, %N, and %organics. The upper organic-rich section (0–7 cm) shows high %S, whereas the lower section (74–79 cm) shows low %S. Two organic-rich horizons are similarly observed in AC3 (44–48cm, 52–60 cm) and also show high %N, %OC, and %organics, although %S values are moderate for both sections. The organic sections in both AC2 and AC3 were confirmed visually by the presence of organic and woody debris and a shift to a darker colour than surrounding sections. AC2 also displays a series of three sections corresponding to facies D, with fine-grained material

that has higher organic matter content than adjacent samples. These three sections (22–30 cm, 66–74 cm, and 111–123 cm) share relatively fine-grain size and moderate %OC, %N, %organics, and %S. Overall, AC3 demonstrates less variation than AC2, and shows an increasing trend with depth in grain size, density, magnetic susceptibility, and C:N, and a decreasing trend with depth in %organics, %OC, and %N. In AC3, %S is relatively consistent throughout the core.

2.3.3.4 Forested alluvial plain cores

The first core (TC1) was collected from a forested alluvial floodplain adjacent to the rerouted channel of Willow River, near its entry point into Willow Lake (Figure 2.6c). In this setting, present-day overbank flooding and sediment deposition occurs during spring freshest, when Willow River has high energy and a high sediment load, and the Mackenzie Delta water levels are near their peak. Visually, there is a clear stratigraphic demarcation point at about 69 cm in TC1 (supporting information, Figure A7), which is mirrored in the analytical parameters for this core (Figure 2.8). The physical and biogeochemical properties of the upper ~70 cm of TC1 are characteristic of Facies B, which reflects coarse-grained sandy sediments that have low %N, %OC, and %organics. This portion of TC1 most closely aligns with the stratigraphic trends seen in AC2, AC3, and the upper 70 cm of AC1, reflecting high energy overbank flooding that has occurred since the rerouting of Willow River. The deeper section of TC1 (69–128 cm depth) is characterized by Facies A and shows a transition to darker, ice-rich sediments with higher %N, %OC, %organics, and %S, which peak at the ~70 cm breakpoint and then decrease with depth. The most basal sample of TC1 (106–128 cm) has a %S value that is much lower than the rest of the core and more closely associated with %S ranges present in TC2; potentially indicative of a shift to a forested environment with little sedimentation associated with historical overbank flooding.

The second core taken from forested alluvial plain (TC2) is located along the shoreline of Willow Lake, distal to the entry point of the re-routed Willow River into the lake. This sample is most proximate to AC1, with deposition occurring in a low-energy environment due to high water levels present in Willow Lake. TC2 is the most visually different from the rest of the cores (supporting information, Figure A8), which is reflected

in the low density, magnetic susceptibility, and %S, and the high %organics, %OC, and %N that characterize this core (Figure 2.8). The upper 25 cm of TC2 show characteristics similar to those of Facies A. This upper section of the core is predominantly composed of organic debris and detrital materials typical of a forest floor, with traces of sandy sediments, and shares characteristics with highly organic sections identified in cores AC2 and AC3. The lower portion of the core (25–84 cm depth) shows characteristics that do not align with any of the identified prograding delta Facies (Facies F) and appears to represent the historic active layer with low sedimentation rates characteristics of stable forested alluvial settings. This portion of TC2 is dominated by coarse-grain size and highly organic materials, with % N, %OC, and %organics continuing to increase with depth. %S shows minor variation with depth and matches low %S values observed in the organic horizons within AC2 (74–79cm) and the basal sample in TC1 (106–128 cm). The stratigraphic characteristics of the lower portion of TC2 closely align with the measured parameters in the upstream active layer sample (H4-AL; Figure 2.7).

2.3.3.5 Lake bottom cores

The most proximal lacustrine core to Willow Lake (LC1), shows low grain size (fine silt) throughout the core. Low %N, %OC, and %organics, which show minor variation with depth (Figure 2.9), and are most similar to the fine-grained materials present in Facies D towards the bottom of AC1. This core shows an increase in %S with depth. A peak in C:N is observed in the middle of the core (10–15 cm depth), similar to LC2 (8–20 cm) and LC3 (6–10 cm, 34 cm). LC2 shows more variation in physical and chemical parameters than LC1, with a higher %OC mid-core (8–20 cm), and an increased grain size observed in the bottom 5 cm of the core (Figure 2.9). However, the parameters throughout LC2 are also similar to the characteristics of Facies D present in AC1. Grain size in LC3 is coarser and more variable than in LC1 and LC2, and %organics, %OC, %N, and %S are more variable throughout the core. In LC3, the general concentration of %N is relatively high compared to the other lake cores, with a minimum value observed at a depth of 6 cm, which aligns with the overall nitrogen signatures observed in the other lake cores. LC3 shows a fining downward sequence in grain size, except for a point of low grain size near the surface of the core (6 cm depth). Overall, LC3 shows a transition at 10 cm depth, with the upper

portion of this core more similar to LC1 and LC2 (Facies D), potentially representing a shift from materials predominantly derived from Willow Lake to materials coming from the Husky and Peel Channels.

Of the three cores, only LC3, the most distal lake in the chain, showed a peak in ^{137}Cs, which occurred at ~15 cm (Supporting information, Figure A9), indicating deposition of this section circa 1963. ^{214}Bi, ^{210}Pb, and ^{214}Pb trends in all lake cores show no discernible patterns, which indicate complex sedimentary processes that preclude the determination of sedimentation rates or sediment core ages.

2.3.3.6 Mineralogy

NMDS analysis of XRD data indicated clear divergence in mineralogical composition across parent material and depositional samples. In general, samples plotting positively along both MDS1 and MDS2 were associated with minerals that are easily weathered, such as dolomite, calcite, sylvite, and pyrite (MDS1) and gypsum, halite, and tremolite (MDS2; Figure 2.10a). In contrast, samples plotting negatively along both axes are dominated by feldspars and minerals resistant to weathering, such as albite and anorthite (MDS1), and orthoclase, Na-bearing anorthite, rutile, and illite (MDS2). The NMDS analysis indicates three groupings of similar mineralogy (Figure 2.10). Most parent materials, including all headwall and scar zone samples, as well as one cut bank sample and one alluvial sample, plot positively along MDS2 and neutrally along MDS1. In contrast to other headwall samples, the H4 active layer sample (H4-AL) plotted negatively along MDS1. A series of alluvial, terrestrial and lake core samples, as well as several cut bank samples, plotted negatively along MDS1 and MDS2. Finally, a series of AC1 samples plotted positively along MDS1, with some positive and negative spread across MDS2. These samples represented a combination of near surface, mid core, and deep core sections. Of the alluvial core samples, this group is most dissimilar to parent materials.

Although the stratigraphic parameters for the upper 70 cm of AC1 align with trends observed in AC2 and AC3, the mineralogical data differs slightly (Figure 2.10b). AC2 and AC3 cluster tightly in MDS space, with AC3 showing slightly more variation than AC2, and plot neutrally along MDS1 and negatively along MDS2. These alluvial samples are closely associated with several cut bank and stream bed samples (CB5, CB8, SB10), as

well as the middle and most basal sections of AC1 (59–120 cm and 244–347 cm, respectively). The upper 41 cm of AC1, as well as the section from 139–244 cm plots more negatively along MDS1, with greater spread along MDS2.

The cores taken from forested alluvium show larger variability in samples that are likely derived from higher energy depositional environments (TC1 surface) compared to lower energy settings (TC1 bottom, TC2). Near-surface terrestrial core samples from TC1 (upper 69 cm) are somewhat more similar to permafrost endmembers than deeper sections within this core (Figure 2.10c), which shift towards high %organics, %OC, and %N observed at the apparent pre-diversion forest floor in this core (Figure 2.8). TC2 samples show minor variation with depth, and plot most closely to cut bank and stream bed samples within MDS space. Lake (gravity) cores show the lowest variability among the analyzed samples (Figure 2.10d). All lake cores (LC1, LC2, and LC3) plot closely to cut bank and stream bed samples (CB2, CB5, CB8, SB10), with the surface sample of LC2 being most like headwall and scar zone parent materials out of the lake core samples.

2.3.3.7 Cations

A PCA of sample cation composition explained 70% of sample variation in the first two principal component axes. All elements plot positively to neutral along PCA1. Samples plotting positively along PCA1 tend to be derived from environments with low depositional energy, such as low energy facies of AC1, low energy forested alluvium samples, lake sediments, and headwall samples (Figure 2.11a). In contrast, coarser materials that are deposited within the high energy environment of the prograding delta of Willow Lake (AC1–AC3), as well as the near surface forested alluvium sample (TC1-12) and several cut bank samples (CB5, 8, 9) plot negatively along PCA1. PCA2 tended to separate cations that are easily weathered (e.g., Ca, Mg) from those that are more stable in soils (e.g., Al, Sr). Non-active layer headwall samples all plot positively along this axis, while active layer and certain cutbank (CB2) samples plot negatively. Core samples associated with low energy depositional environments (stable forested alluvium, lake sediments) also plot negatively on PCA2.

Similar to the trends seen in the NMDS for XRD samples (Figure 2.10), AC2 and AC3 show modest variation in ordination space. These samples plot negatively along PCA1 and neutrally along PCA2 (Figure 2.11b) and are closely related to several cut bank samples (CB5, CB8, and CB9). Surface samples from AC1 (6–70 cm), as well as a mid depth section (244–270 cm) also plot closely to AC2 and AC3. Mid section samples from AC1 (88–142 cm; 224–244 cm) are most similar to non-active layer headwall samples, while the remaining AC1 samples (155–224 cm; 210–244 cm; 270–358 cm) are most similar to the upstream active layer (H4-AL) and stream bed (SB10) parent materials. Thus, variation within AC1 may be due to variations in energy, surface exposure, weathering, and soil development reflective of this dynamic depositional environment.

Forested alluvium core samples show variation with depth. The surface sample of TC1 is more similar in cation composition to AC2 and 3, as well as several cut bank samples, all of which are reflective of higher energy settings and mineral-rich deposits. This aligns with trends seen in the stratigraphic parameters of this core (Figure 2.8), as well as patterns in mineralogy (Figure 2.10). In contrast, the basal sample from TC1 is more closely associated with TC2 samples, as well as H4-AL and CB2 (Figure 2.11c). All lake core samples are also closely aligned with these samples, but notably the basal sample from LC2 is most closely associated with SB-10 (Figure 2.11d). The samples in this grouping represent either low energy depositional environments, or relatively stable terrestrial environments.

2.3.3.8 Radiocarbon

Parent materials (headwall, scar zone, and cut bank samples) show the most depleted $\Delta^{14}C$ values ((-878.7) – (-994.9) ± 0.7 ‰; -909.3 ± 0.7 ‰; -848.0 ± 0.7 ‰; respectively) and are relatively similar in values, barring H4-AL, which is the most $\Delta^{14}C$ enriched of all the samples analyzed (-75.8 ± 1.4 ‰). The $\Delta^{14}C$ values for Willow Lake alluvial samples and gravity core sediments lie within the range of parent materials (Table 2.6; Figure 2.12). Surface samples from LC2 and LC3 are more $\Delta^{14}C$ depleted than samples at depth, with the surface sample of LC2 (value) approaching $\Delta^{14}C$ values observed for headwall (H8-Pl) and scar zone (SZ4) samples. Similarly, surface samples from AC1 are more $\Delta^{14}C$ depleted than samples at depth, barring AC1-282, which is the

most $\Delta^{14}C$ depleted sample within this core. The remaining alluvial samples from Willow Lake (AC2 and AC3) show the opposite trend, with surface samples more $\Delta^{14}C$ enriched than samples at depth.

Overall, samples more enriched in $\Delta^{14}C$ also displayed higher %OC values (Figure 2.12b). H1-AL has the highest %OC and the most enriched $\Delta^{14}C$ value, whereas headwall, scar zone, and cut bank samples were universally low in %OC relative to alluvial samples. Lake core samples tended to have higher %OC than alluvial samples, except for AC2-74 and AC3-106, suggesting contemporary additions of OC, which is consistent with radiocarbon results. When looking at N:C values, permafrost derived parent materials (non-active layer headwall and scar zone samples) show higher values when compared to cut bank and active layer parent materials (Figure 2.7, Figure 2.12a). The most $\Delta^{14}C$ enriched core samples (AC2-74 and AC3-106) are most like active layer and cut bank samples. The remaining alluvial and lake core samples show depletion in N:C relative to permafrost derived parent materials, except for AC1-282, which closely aligns with $\Delta^{14}C$ and N:C values for these parent materials, and LC3-25, which is the most like SZ4 in terms of N:C value.

2.4 Discussion

Within the Willow River catchment, the density and area of thaw-induced mass-wasting features have increased since 1986, with the majority of identified disturbances lying within the glacial limit of the LIS (Figure 2.3). Within the western Canadian Arctic, glacial conditioning, changing hydroclimatic regimes, and variation in geomorphic setting all influence the distribution and observed rapid increase in thaw-driven mass wasting (Kokelj et al., 2021; Kokelj, Lantz, et al., 2017). The permafrost preservation of relict ground ice throughout glaciated portions of the Willow River catchment has predisposed the terrain to thaw-driven geomorphic modification (Kokelj, Lantz, et al., 2017), reflecting early-stage post glacial erosional processes and sediment mobilization (Ballantyne, 2002). The increasing magnitude of disturbance area has increased slope-to-stream connectivity, which is reflected by increased levels of turbidity in lakes directly affected by thaw slumping, and in Delta lakes tens of kilometers downstream of thaw-driven mass-wasting features. The most dramatic example of the rejuvenation of the post-glacial

sediment cascade (Kokelj, Lantz, et al., 2017) is the near complete infill of Willow Lake with sediments. The development of a prograding delta within Willow Lake, and the changes in physical and biogeochemical properties of deposited sediment, highlight that increased sedimentation from accelerated thaw-induced mass wasting has the potential to shift ecosystem function within aquatic systems. Materials deposited within Willow Lake, which would have otherwise transited further downstream, can have implications for biogeochemical and ecological processes at various scales.

2.4.1 Interactions between landscape history and climate intensify patterns of thaw-induced mass-wasting features

The Peel Plateau-Richardson Mountain region is a hot-spot of geomorphic activity within the western Canadian Arctic (Kokelj, Lantz, et al., 2017), and within this region, thaw-driven mass wasting in the Willow River catchment is particularly pronounced (Kokelj et al., 2021; Lacelle et al., 2015). The rapid, non-linear evolution of mass-wasting features in this study reiterates these findings. The general lack of disturbance in the western-most reaches of the catchment is consistent with glacial conditioning and processes associated with positioning of the LIS during the Last Glacial Maximum. The preservation of relict ground ice (basal glacier ice and segregated ice) following LIS retreat makes this area particularly susceptible to landscape disturbance as climate continues to change (Kokelj, Lantz, et al., 2017; Lacelle et al., 2015). In addition to the glacial history of this area, the high elevation and moderately steep slopes characteristic of the foothills of the Richardson Mountains make the Willow River catchment more susceptible to the development of thaw-driven mass wasting due to terrain instability caused by the ice-preserved fluvially-incised setting when compared to inland plain environments (Kokelj, Lantz, et al., 2017; Lacelle et al., 2015).

Layered on top of glacial conditioning and watershed topography, increasing temperatures and precipitation throughout the study period may interact with each other and drive sediment excavation, which further enables slump growth (Kokelj et al., 2015; Lacelle et al., 2010, 2015). This region has experienced a ~2.5 °C increase in mean annual temperature over the last several decades (Figure 2.2a), which is greater than most other Arctic locations (Overland et al., 2011). Similarly, amounts of total and extreme

precipitation are generally higher in the western Canadian Arctic when compared to other locations in the north (Yu & Zhong, 2021). The high densities of disturbance observed in this study may be exacerbated by increases in debris tongue number and area, because the development of debris tongues can cause the initiation of mass-wasting features in adjacent areas due to the development of thaw-induced stream blockages, which can raise water levels, divert water flow, and induce thermoerosion on adjacent slopes (Kokelj et al., 2015).

2.4.2 Thaw-induced coupling of slopes to streams impacts downstream lake turbidity

The increasing number and area of debris tongues identified within the Willow River catchment have caused terrestrial environments to be increasingly connected to the aquatic system over our 30-year study period. This coupling of slopes to recipient streams means that the large amount of sediment that can be displaced from thaw-induced mass wasting now has a higher potential to impact downstream aquatic systems (Kokelj et al., 2015). The ability for stream networks to transport slump-excavated materials is dependant upon the transport capacity of the stream, which can regulate the degree to which materials deposited within valley bottoms are mobilized downstream (Shakil et al., 2020). Streams that are impacted by thaw-driven mass wasting can have sediment concentrations that are two orders of magnitude higher than in unimpacted systems (Kokelj, Lantz, et al., 2017; Kokelj, Tunnicliffe, et al., 2017; Shakil et al., 2020). Prolonged periods of high sediment transport to downstream aquatic environments can cause geomorphic shifts to the fluvial network, such as the rerouting of the main stem of Willow River observed here (Kokelj et al., 2013, 2021), and can cause substantial biogeochemical (Shakil et al., 2020; Zolkos et al., 2018) and ecological (Chin et al., 2016) effects.

This study shows a substantial effect of thaw-driven geomorphic change on lake water turbidity, showcasing increases in turbidity in all but abandoned channel lakes. Of the broad lake categories that experience increasing NDTI trends, the within-catchment lakes showed the greatest overall increase, which aligns with findings from previous work showing that thermokarst initiation and subsequent sediment mobilization result in

elevated turbidity levels in impacted lakes (Lewkowicz & Way, 2019; Roberts et al., 2017). In contrast to previous work, which found that 95% of lakes with elevated turbidity experienced nearshore geomorphic activity (Lewkowicz & Way, 2019), most impacted lakes within the Willow River catchment are located more than 10 km downstream of the nearest identified thaw-driven mass-wasting feature. This may be due to the high density of disturbance within the catchment, and the increased connectivity between slopes and streams, which allows for a more integrative composition of sediment from multiple sources of thaw-driven mass-wasting to reach downstream lakes (Kokelj et al., 2021; Lacelle et al., 2010). Elevated NDTI within the Husky Channel lakes indicates broad changes within the landscape, highlighting the ability for thaw-driven mass wasting effects to propagate through aquatic networks, and the breadth of disturbance in this region.

2.4.3 Thaw-driven sedimentary effects archived in depositional environments

The rerouting of Willow River has reconfigured sediment delivery and energy environments within Willow Lake, indicated by grain size. The alluvial cores that are more proximal to the river inflow channel within Willow Lake are composed of coarser-grained material, and a clear transition from coarser-grained material at ~70 cm to finer-grained materials at depth within AC1 appear to mark the transition from a high to low energy depositional environment with progradation of the delta front. This is also clearly observed in TC1, which shows a downward transition from coarse-grained materials that are low in organic content, likely derived from high energy flooding events along the rerouted channel of Willow River, to fine-grained, more organic rich materials at depth. Mackenzie Delta lakes that have historically been supplied with sediments from both the Husky Channel and Willow River tend to display this coarsening upward sequence in sediment grain size (~5 μm near surface, ~2 μm at depth) and a low percentage of organics (~5%; Lattaud et al., 2021; Mesquita et al., 2010; Michelutti et al., 2001). This coarsening upward sequence reflects rerouting and progradation of the rapidly growing Willow Lake delta. Coarser materials were initially deposited where the rerouted river entered Willow Lake, with inflowing finer-grained materials being deposited distally along the growing delta front, or in adjacent connected lakes (Gilbert, 1885, 1890; Kostic & Parker, 2003). Coarser-grained materials build up on surfaces adjacent to the inflow channel and delta

plain. The coarse-grained materials that are present within the upper ~70 cm of AC1, as well as throughout the depths of AC2 and AC3, correspond with high energy environments typical of a prograding delta. As well, the shift to finer grained materials below ~70 cm in AC1 likely illustrates the earlier deposition of fine-grain materials along the lower energy environment when the site was still proximal to the delta front. These materials overlay historic lakebed sediments (found below 270 cm in AC1), which are similar in grain size, but show variations in other core parameters.

Variation in parameters such as grain size and %OC for alluvial cores taken from within the prograding delta of Willow Lake, as well as from the forested alluvial cut bank surface along the rerouted channel of Willow River, may be explained by the dynamic interplay of discharge and sediment load of Willow River with the rise and fall of flood waters in the Mackenzie Delta (Willow Lake). Within a prograding delta in a lake basin, sediment that lies above the water level has significantly greater organic content and significantly larger grain size (Shields et al., 2019). Exposed lake bottom sediments, either due to lake drainage or infill caused by high sedimentation (such as seen within Willow Lake), can have implications for climate feedbacks. Drained lake basins are often a carbon sink, with a larger proportion of permafrost-derived carbon being stored within lake sediments rather than being released to the atmosphere (Anthony et al., 2014). Vegetation regrowth and expansion along the exposed sediments has the potential to further sequester legacy carbon (Turetsky et al., 2020). Additionally, the exposure of alluvial sediments can result in a negative climate feedback due to an increased albedo caused by the shift from darker surface waters to lighter, more reflective sediments (Jones et al., 2022; Webb et al., 2022). Increased sedimentation within Arctic lakes to the point of infill can also contribute to the recently reassessed estimates of declining surface area of Artic lakes (Kokelj et al., 2015, 2021; Lacelle et al., 2010; Lewkowicz & Way, 2019; Webb et al., 2022), which can further impact the ecological role of Arctic lakes and climate feedbacks, as well as impact Northern communities and local land users. The role of this succession in broad scale sedimentary, fluvial, and biogeochemical regimes warrants further investigation in future studies.

In terms of their mineral and cation composition, alluvial materials appear to separate based on depositional energy, with materials that are relatively resistant to weathering found in high energy environments. Minor mineralogical and elemental deviations from the identified core facies, which were based on the stratigraphic parameters for alluvial deposits within Willow Lake and flooded overbank alluvium, are justified by variations in depositional energy and sample processing prior and during deposition. Permafrost parent materials are mostly composed of aluminosilicate and sulfate minerals that are highly susceptible to weathering processes and generally align with mineralogical compositions of permafrost found in catchments ~80 km south of the study site (Malone et al., 2013; Zolkos & Tank, 2020). In contrast, core samples from higher energy environments are more similar to cut bank samples in terms of compositional makeup, rather than permafrost parent materials. While changing climate may increase riverbank erosion (Chalov et al., 2021), in-situ processing may also enable exposed alluvial materials to be more compositionally similar to highly eroded cut bank materials, for soil development has been documented in subaerial sediments within prograding deltas (Bevington & Twilley, 2018; Shields et al., 2019). High elevation alluvial samples within Willow Lake (AC2 and AC3), as well as sediments that are frequently subaerial (surficial AC1), are likely to have experienced diagenetic alteration prior to deposition and are now undergoing in-situ processing (Shields et al., 2019). These findings indicate that sediments liberated by thaw-driven mass wasting are susceptible to dynamic contemporary processes that may result in ongoing biogeochemical processing and a succession of chemical composition within deposited sediments.

Analysis of parent materials aligns with previous work that shows that particulate permafrost materials in the region are generally recalcitrant (Bröder et al., 2021; Shakil et al., 2020). Alluvial and aquatic core samples fall within the boundaries set by the active layer and permafrost samples for %OC, N:C, and $\Delta^{14}C$ values, but with opposing patterns observed for alluvial and lake cores. Alluvial core samples from AC2 and AC3 tend to show that relatively younger, more biogenic, and more labile materials are found near the surface of the cores, with older materials more similar to non-active layer parent materials at depth. This may indicate that sedimentation is occurring from a combination of sources, including materials from relatively younger and more biogenic cut banks and active layers

(Bröder et al., 2021; Shakil et al., 2020, 2022), or that there is potential for post-depositional processing (Feng et al., 2015). Given that the surficial samples from AC2 and AC3 were characterized by Facies A (with visible organic matter incorporation) and Facies C (very fine sand, limited to no organics visible), respectively, it appears that both processes may be present.

In contrast to alluvial cores AC2 and AC3, core AC1 was more consistently aged, though with characteristics that are consistent with varying sources. At depth, higher N:C and %OC values, and more depleted $\Delta^{14}C$ values, are consistent with historical lakebed samples, whereas the surficial AC1 sample with relatively depleted N:C and %OC values is representative of fine-grained materials deposited along the delta front within Willow Lake following river reroute. Lacustrine cores show opposing $\Delta^{14}C$ patterns when compared to alluvial cores, with surface materials that were more $\Delta^{14}C$ depleted and carbon enriched than materials found at depth, implying that these lakes have transitioned to have increasingly less modern within-lake primary production, with increased inputs from Willow River. LC2-08 is the only lake core sample that is more $\Delta^{14}C$ depleted than non-permafrost parent materials. In concert with the lack of ^{137}Cs within LC1 and 2, this finding strengthens the interpretation that the upper 20 cm of LC2, and likely all of LC1, are dominated by sediments that have travelled from Willow Lake following the river reroute. Of the remaining lake core samples, LC3-25 is relatively N:C enriched compared to all other samples, barring SZ4. This result may indicate the incorporation of petrogenic organic carbon that is different from permafrost materials, and highlights that the bottom half of LC3 likely has minimal incorporation of Willow River derived permafrost materials.

2.4.4 The Mackenzie Delta is a long-term sedimentary sink

In addition to having a coarser grain size, materials that are deposited within the alluvial surface of Willow Lake tend to be low in percent carbon, nitrogen, sulfur, and organics compared to materials found at depth within AC1, but (when not exposed to conditions that allow for in situ processing) show elevated concentrations of mineral substrate that is resistant to weathering. Decreased organic content and nutrients have been observed in several studies that analyze the impacts of upstream permafrost thaw on lake water and sediments, showing substantial differences between thermokarst

impacted lakes compared to undisturbed water bodies (Koeklj et al 2005 Bowden et al., 2008; Mesquita et al., 2010; Thompson et al., 2012; Vonk, Tank, Mann, et al., 2015). These trends, which closely align with the observed signatures in analyzed permafrost parent materials, indicate a shift in sediment transport and lake sediment deposition that can have impacts on ecological functioning within streams and lakes (Blaen et al., 2014; Chin et al., 2016; Murdoch et al., 2021; Schuur et al., 2015; Vucic et al., 2020).

Currently, the majority of sediment from Willow River is captured and deposited within Willow Lake, highlighting the potential for permafrost-mobilized materials to be redeposited and placed within long-term storage. However, it is clear when looking at the NDTI and sediments of rerouted-sampled lakes, as well as the NDTI of Husky Channel lakes, that a proportion of thaw-induced mass wasting materials are moving further downstream, which are likely being incorporated within larger riverine systems (i.e., the Peel and Mackenzie Rivers). The depositional environment within Willow Lake allows us to capture and measure materials that would otherwise move downstream and undergo ongoing weathering of mineral surfaces in transit (Zolkos et al., 2018), which would impact biological processing (Shakil et al., 2022), and have large scale effects on water quality, lake community structure and function, and microbial production within impacted aquatic systems (Droppo et al., 2022).

2.5 Conclusion

It is important to consider various landscape characteristics when investigating the biogeochemical response of aquatic systems to permafrost thaw, such as geologic legacy, the physical and geochemical nature of permafrost, and the mechanisms of downstream transport (Tank et al., 2020). Within the Willow River catchment, the influence of glacial legacy on the physical characteristics of permafrost, the rapid rate of climate change, and the steeply-incised hillslope terrain make the lower two-thirds of the catchment particularly vulnerable to a rapid increase in the number and magnitude of thaw-induced mass-wasting features (Figure 2.3a; Kokelj et al., 2021; Kokelj, Lantz, et al., 2017; Lacelle et al., 2010, 2015). An increase in connectivity between terrestrial and aquatic systems has substantially augmented sediment mobilization by streams, which has resulted in a cascade of downstream effects that have impacted fluvial and

sedimentary systems and the biogeochemical processes that these environments host. Changes in river geomorphology within the Willow River catchment, induced by accelerated thaw-induced mass wasting, resulted in the rerouting of the main river channel through Willow Lake (Kokelj et al., 2021). Thaw-derived sediments that would otherwise continue further downstream have been captured within Willow Lake, highlighting that materials mobilized by permafrost thaw can be redeposited and placed back into long term storage. The resulting shift from dark surface waters to lighter exposed sediments within Willow Lake can have implications to climate feedbacks (Anthony et al., 2014; Turetsky et al., 2020). The fine-grained materials that are not captured and deposited within Willow Lake become available to cascade further downstream, as evidenced by elevated NDTI, and can impact the ecological functioning of aquatic systems at broad scales within North America's largest delta (Blaen et al., 2014; Chin et al., 2016; Droppo et al., 2022; Schuur et al., 2015; Vucic et al., 2020). Systems such as Willow Lake should be considered when predicting the cascading effects of permafrost thaw, developing Arctic climate projections, and preparing local communities for future changes in climate.

2.6 Tables

Table 2.1 Characteristics of identified lake categories.

Zone	Source	N	Mean Area (ha)	Median Area (ha)	StDev Area (ha)
Upland	Colluvial and moraine	29	4.128	2.250	4.679
Abandoned	Alluvial	29	11.042	2.340	22.011
Rerouted	Alluvial and fluvial	35	12.479	4.950	25.368
Rerouted-sampled	Alluvial and fluvial	4	46.103	15.750	61.551
Husky	Alluvial and colluvial	24	18.701	8.460	24.686

Table 2.2 Parent material categories and descriptions.

Sample ID	Category	Description
H4-AL	Headwall	Near-surface active layer sample from retrogressive thaw slump H4
H4-Ho1	Headwall	Holocene layer permafrost sample from retrogressive thaw slump H4
H4-Ho2	Headwall	Holocene layer permafrost sample from retrogressive thaw slump H4.
H4-Pl1	Headwall	Pleistocene layer permafrost sample from retrogressive thaw slump H4.
H4-Pl2	Headwall	Pleistocene layer permafrost sample from retrogressive thaw slump H4.
SZ4	Scar zone	Scar zone surface sample from retrogressive thaw slump H4.
H7	Headwall	Sample from eroding colluvial landslide feature H7.
H8-Pl	Headwall	Pleistocene layer permafrost sample from retrogressive thaw slump H8.
SZ8	Scar zone	Scar zone surface sample from retrogressive thaw slump H8
CB2	Cut bank	Cut bank sample from centre of the eroding landslide. Located upstream of all other parent materials.
CB5	Cut bank	Sample from eroding cut bank downstream of retrogressive thaw slum H4.
CB8	Cut bank	Sample from eroding cut bank downstream of retrogressive thaw slump H8.
CB9	Cut bank	Sample from eroding cut bank upstream of Willow Lake.
SB10	Cut bank	Sample from depositional surface downstream of Willow Lake.

Table 2.3 Characteristics of core facies identified in alluvial cores. Cryostructure classified based on Murton and French (1994).

Facies	Characteristics
A	High organic content (wood), low magnetic susceptibility, low density, variable grain size (coarse sand to silt 10–1000 μm) little to no ice content visible, thin wavy lenticular cryostructure, Munsell colour 7.5YR 5/4 to 7.5YR 5/2.
B	Coarse-grained (very fine sand to coarse sand 50–1000 μm), visible horizontal laminations, high density, moderate magnetic susceptibility, little to no ice content visible, structureless cryostructure, Munsell colour 5YR 7/4 to 7.5YR 4/3.
C	Medium-grained (very fine sand 50–100 μm), visible horizontal laminations, high density, high magnetic susceptibility, minor ice content, thin non-parallel planar lenticular cryostructure, Munsell colour 7.5YR 7/2 to 7.5YR 6/4.
D	Fine-grained (silt 2–50 μm), dark horizontal laminations visible, moderate ice content, thin reticulate cryostructure present, Munsell colour 7.5YR 6/2 to 5YR 5/1.
E	Very fine-grained (clay to silt 0–50 μm), no clear laminations, major ice content, thick reticulate cryostructure present, Munsell colour 5YR 8/2 to 5YR 6/1.
F	Purely organics. Little to no ice content present, structureless cryostructure, Munsell colour 7.5YR 3/2 to 7.5YR 3/4.

Table 2.4 Outputs of mixed effects models to assess changes of turbidity over time within lake categories. Results show the slope estimate, standard error, t-value and the upper and lower 95% confidence intervals on the slope estimate for each lake category. Note that the samples lakes are a subset of the rerouted lake category.

Category	Estimate (10^{-3})	Standard error (10^{-3})	t-value	95% CI Lower (10^{-3})	95% CI Upper (10^{-3})
Upland	1.399	0.158	8.848	1.089	1.710
Abandoned	-0.405	0.289	-1.399	-0.973	0.164
Rerouted	1.302	0.183	7.117	0.943	1.661
Sampled	1.895	0.482	3.935	0.936	2.855
Husky	0.880	0.184	4.779	0.518	1.242

Table 2.5 Outputs of break point analysis conducted to assess significant changes in turbidity trends over time showing slope estimate, standard error, t-value, and the upper and lower 95% confidence intervals for each segmented relationship identified by lake zone. Note that the samples lakes are a subset of the rerouted lake category.

Category	Year range	Estimate (10^{-3})	Standard error (10^{-3})	t-value	95% CI Lower (10^{-3})	95% CI Upper (10^{-3})
Upland	1986–2017	1.977	0.263	7.504	1.458	2.496
Upland	2017–2022	-3.598	1.615	-2.228	-6.780	-0.417
Abandoned	1986–2007	3.002	0.935	3.212	1.160	4.844
Abandoned	2007–2017	-17.101	3.779	-4.525	-24.547	-9.655
Abandoned	2017–2022	7.117	3.023	2.354	1.160	13.074
Rerouted	1986–1996	2.861	3.655	0.783	-4.334	10.056
Rerouted	1996–2022	0.868	0.475	1.827	-0.067	1.802
Sampled	1986–1996	6.369	4.240	1.502	-2.347	15.086
Sampled	1996–2007	-2.974	7.114	-0.418	-17.599	11.650
Sampled	2007–2022	4.303	3.875	1.110	-3.663	12.268
Husky	1986–2001	-0.267	0.673	-0.397	-1.594	1.061
Husky	2001–2022	1.641	0.673	2.439	0.314	2.969

Table 2.6 Radiocarbon (^{14}C) values in years before present (yr BP), fraction modern radiocarbon ($F^{14}C$), depleted radiocarbon ($D^{14}C$), and absolute radiocarbon ($\Delta^{14}C$), with associated error ranges, as well as calibrated age ranges in years before present (cal yr BP).

ID	^{14}C yr BP	±	$F^{14}C$	±	$D^{14}C$ ‰	±	$\Delta^{14}C$ ‰	±	cal yr BP
AC1-88	16895	45	0.1221	0.0007	-877.94	0.69	-879.00	0.69	20530 - 20289
AC1-244	10690	26	0.2643	0.0009	-735.73	0.85	-738.02	0.85	12738 - 12676
AC1-282	18305	54	0.1024	0.0007	-897.59	0.69	-898.48	0.69	22392 - 22116
AC2-74	3031	14	0.6857	0.0012	-314.34	1.20	-320.29	1.20	3257 - 3170
AC2-111	12364	30	0.2146	0.0008	-785.42	0.80	-787.29	0.80	14549 - 14182
AC3-106	8165	20	0.3619	0.0009	-638.13	0.91	-641.27	0.91	9137 - 9015
AC3-135	10066	24	0.2856	0.0009	-714.37	0.85	-716.85	0.85	11752 - 11460
LC2-8	17328	48	0.1157	0.0007	-884.35	0.69	-885.35	0.69	21029 - 20781
LC2-20	7805	20	0.3785	0.0009	-621.54	0.93	-624.83	0.93	8607 - 8541
LC3-6	10031	24	0.2869	0.0009	-713.13	0.85	-715.62	0.85	11653 - 11393
LC3-25	5480	16	0.5055	0.0010	-494.48	1.04	-498.86	1.04	6305 - 6275
H8-PI	16875	48	0.1224	0.0007	-877.63	0.73	-878.69	0.73	20515 - 20269
CB8	15065	38	0.1533	0.0007	-846.70	0.72	-848.03	0.72	18626 - 18474
H4-PI1	40899	733	0.0061	0.0006	-993.85	0.56	-993.90	0.56	45198 - 42841
H4-Ho1	42362	872	0.0051	0.0006	-994.87	0.56	-994.92	0.56	47043 - 43371
H4-AL	563	12	0.9323	0.0014	-67.74	1.43	-75.83	1.43	559 - 537

2.7 Figures

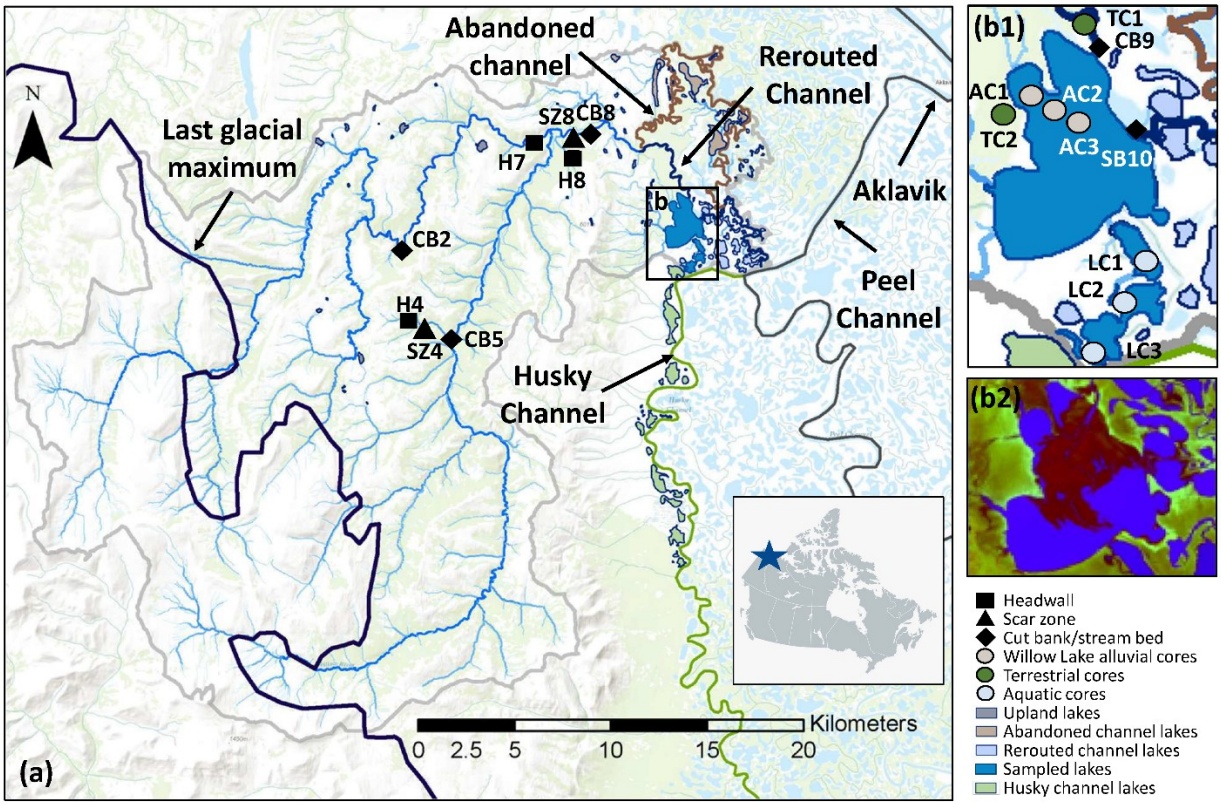

Figure 2.1 Map of the Willow River catchment study area (a). A zoomed in view of the sampled delta lakes and sampling locations (b1) and a tasseled cap transformed image of Willow Lake (2022) highlighting sediment input within the lake in red (b2). The catchment boundary is shown in grey, and the Willow River is shown in blue, with thinner lines illustrating lower Strahler stream order. The base map is from ESRI ArcGIS Online.

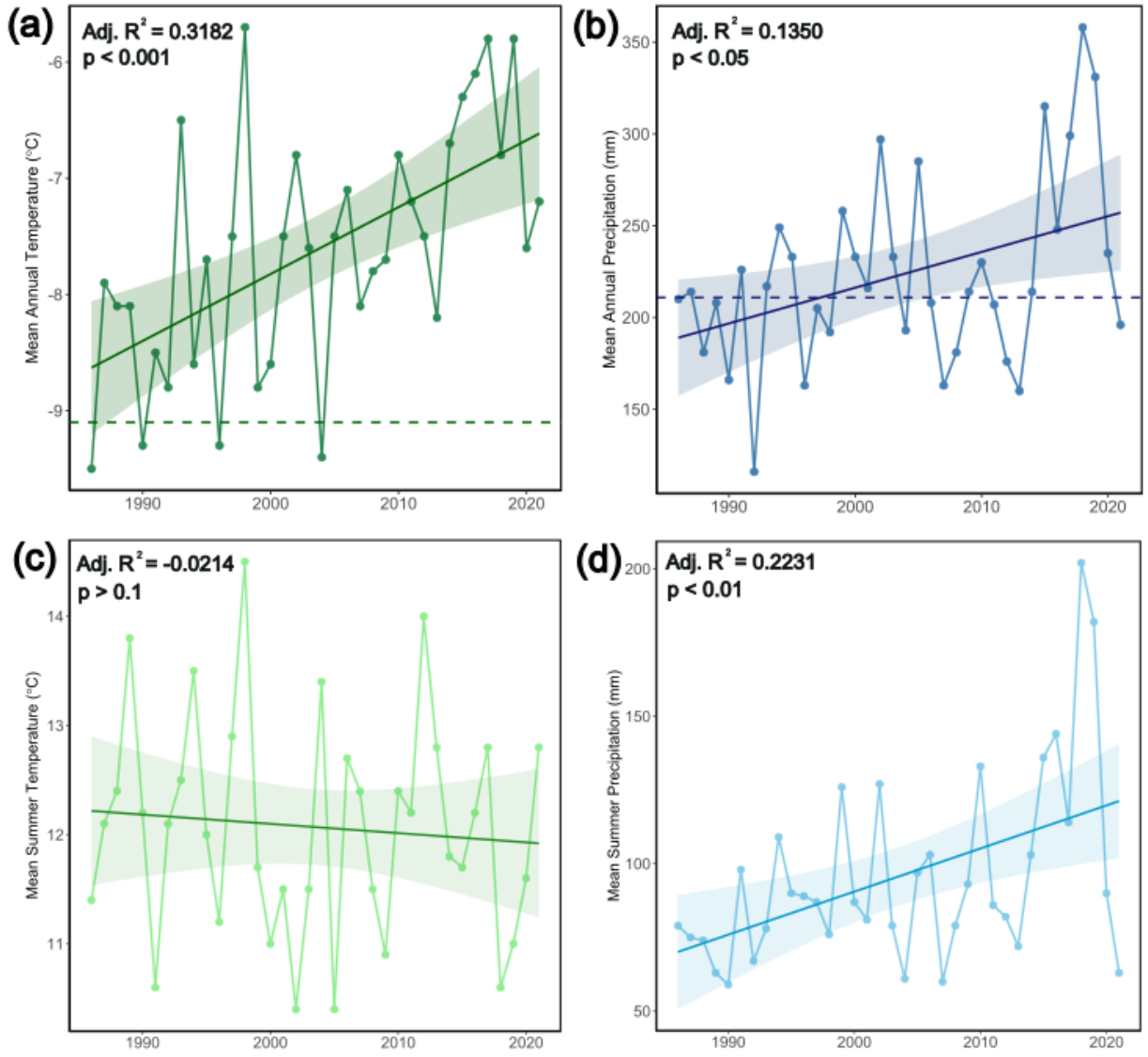

Figure 2.2 Reanalysis climate data for the Aklavik area from 1986 to 2021. The normal trend (1961–1990) is shown by the horizontal dashed line for mean annual temperature (-9.1 C, a) and mean annual precipitation (211 mm, b). Mean summer trends (June–August) are shown for temperature (c), and precipitation (d). The linear trend is shown by the solid line (annual temperature: *y=0.058x – 122.985*, annual precipitation: *y=1.9467x – 3677.1943,* summer temperature: *y=-0.008x + 29.062*, summer precipitation: *y=1.461x – 2831.455*), with 95% confidence intervals indicated via shading.

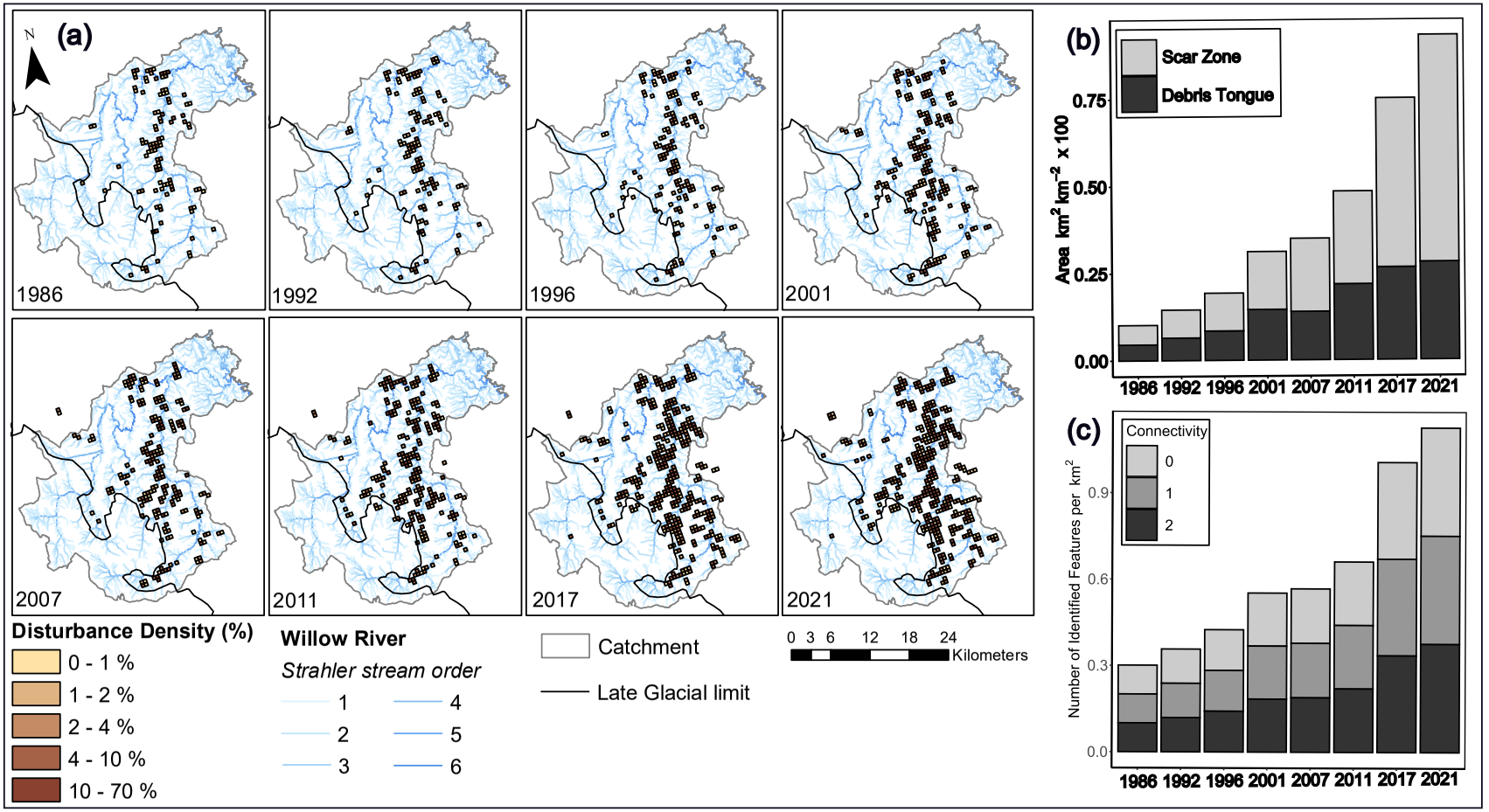
(a)
N
1986
1992
1996
2001
2007
2011
2017
2021
Disturbance Density (%)
0 - 1 %
1 - 2 %
2 - 4 %
4 - 10 %
10 - 70 %
Willow River
Strahler stream order
1
2
3
4
5
6
Catchment
Late Glacial limit
0 3 6 12 18 24
Kilometers
(b)
Scar Zone
Debris Tongue
Area km^2 km^{-2} x 100
0.00
0.25
0.50
0.75
1986 1992 1996 2001 2007 2011 2017 2021
(c)
Connectivity
0
1
2
Number of Identified Features per km^2
0.0
0.3
0.6
0.9
1986 1992 1996 2001 2007 2011 2017 2021

Figure 2.3 The temporal evolution of slump density from 1986–2021, with panels showing disturbance density within individual 500m by 500m cells (a). The temporal evolution of debris tongue and scar zone area from 1986–2021as km^2 feature area per km^2 of catchment area (b). The temporal evolution of slope-to-stream connectivity from 1986–2021, showing features with no (0), adjacent (1), and direct (2) connection to the aquatic network (c).

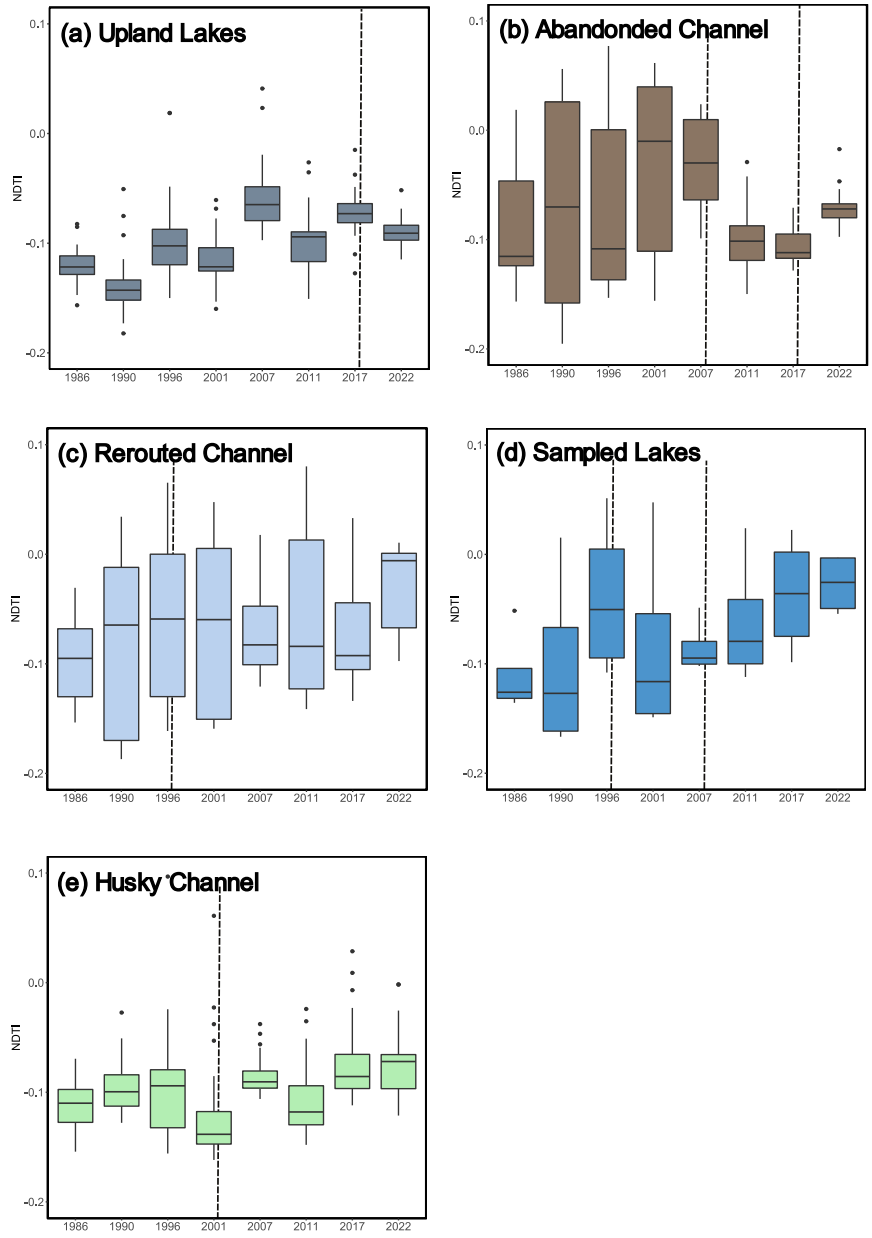

Figure 2.4 Temporal evolution of lake turbidity represented as Normalized Difference Turbidity Index (NDTI). NDTI increases with turbidity. Lakes are classified by category based on inflow and geographic location within the Willow River catchment and surrounding areas: (a) upland lakes, (b) abandoned channel, (c) rerouted channel, (d) sampled lakes , and (e) Husky Channel. Vertical dashed lines indicate shifts in turbidity trends. Demarcation of lake categories is shown in Figure 2.1; results of trend and break point analysis are shown in Tables 3.2 and Table 3.3.

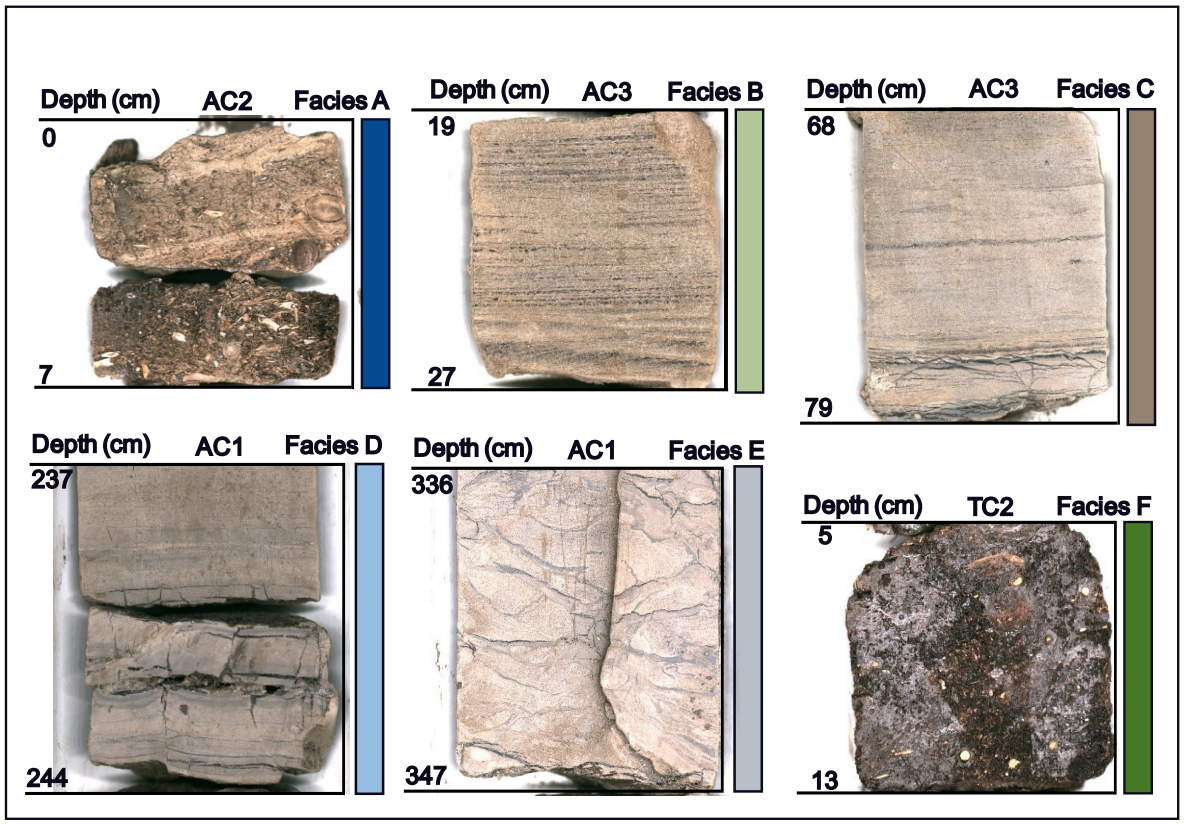

Figure 2.5 High-resolution images of core sections representing facies described in Table 2.1. Facies A (high organic content) is represented by AC2 section 0–7.5 cm. Facies B (coarse-grained, b) is illustrated with AC3 section 19.5–27.5 cm. Facies C (medium-grained) is shown by AC3 section 68.5–79.5 cm. Facies D (fine-grained) is shown by AC1 section 237–244.5cm. Facies E (very fine-grained) is shown by AC1 section 336.5–347 cm. Facies F shows an example of the upper portion of TC2, which is highly organic but likely has some influence from Willow Lake flooding. Facies F is a reference facies that is not observed in the prograding surface of Willow Lake. Complete facies characterization of all cores can be found in supporting information (Figures A4-A8).

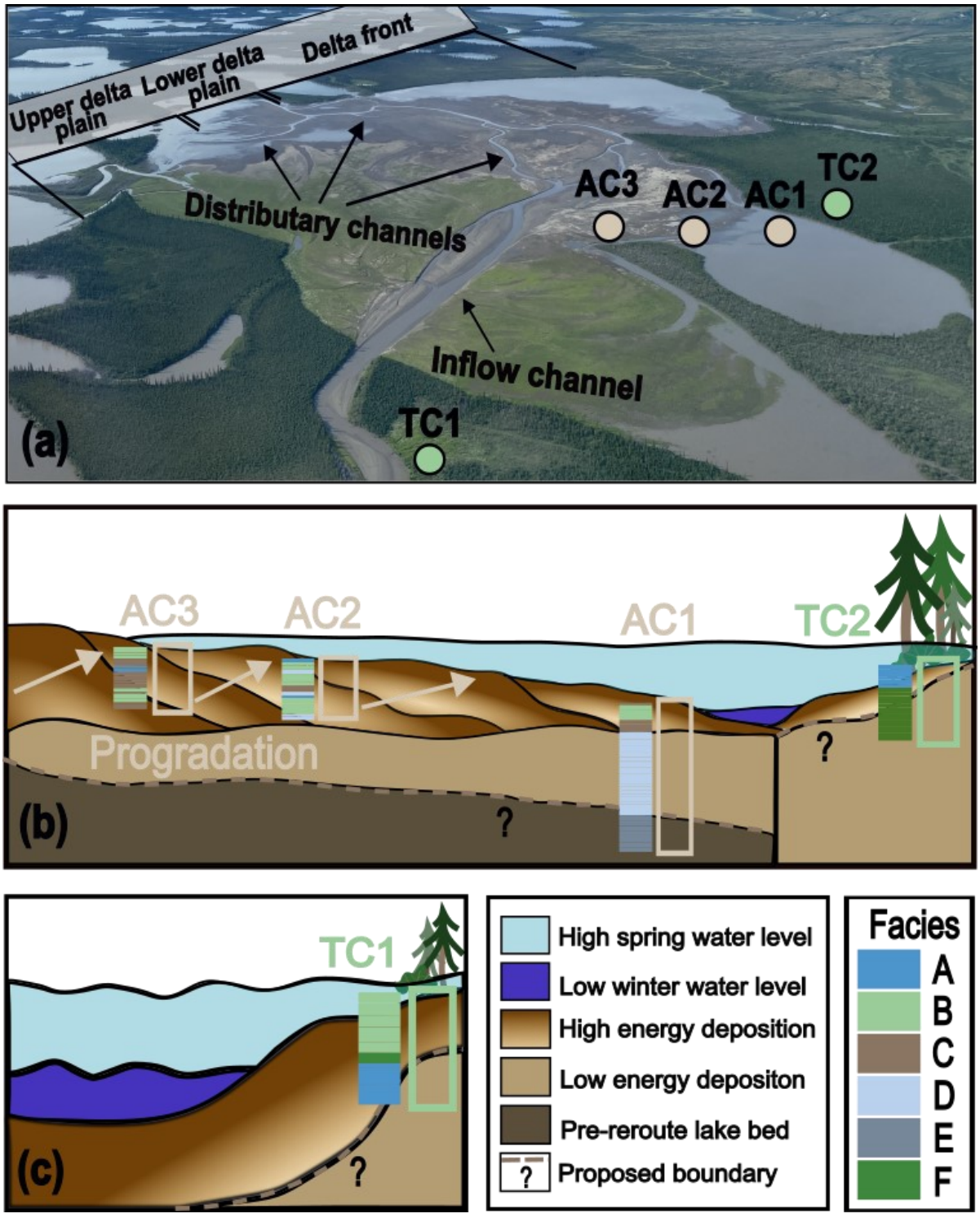

Figure 2.6 Alluvial surfaces within and around Willow Lake. Labeled prograding delta within Willow Lake (a) and the locations of alluvial cores and identified facies within a cross sectional diagram of the prograding delta within Willow Lake (b), and along a cut bank within Willow River at the inflow to Willow Lake (c).

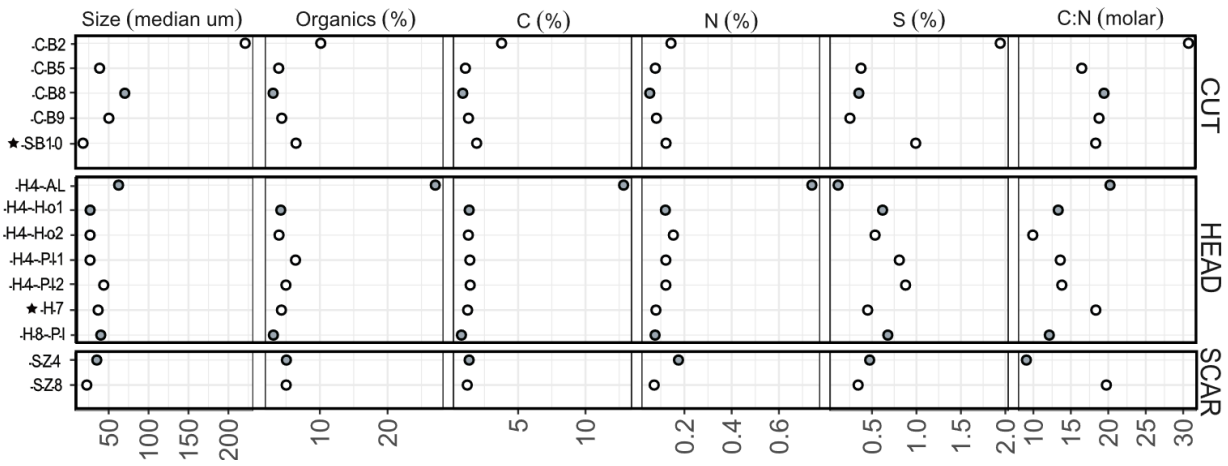

Figure 2.7 Stratigraphic diagrams for parent materials including cutbank (CUT), headwall (HEAD), and scar zone (SCAR) samples. From left to right, parameters are median grain size by percent volume (um), percent mass carbon, percent mass nitrogen, percent mass organics, percent mass sulfur, and the molar ratio between carbon and nitrogen. White points show samples analyzed for X-ray diffraction (XRD), grey points show samples analyzed for radiocarbon ($\Delta^{14}C$) and XRD, and black points show the remaining samples. Samples with a black star next to them (SB10 and H7) indicate that the parent material category doesn't perfectly reflect the sample type, but is the most reflective.

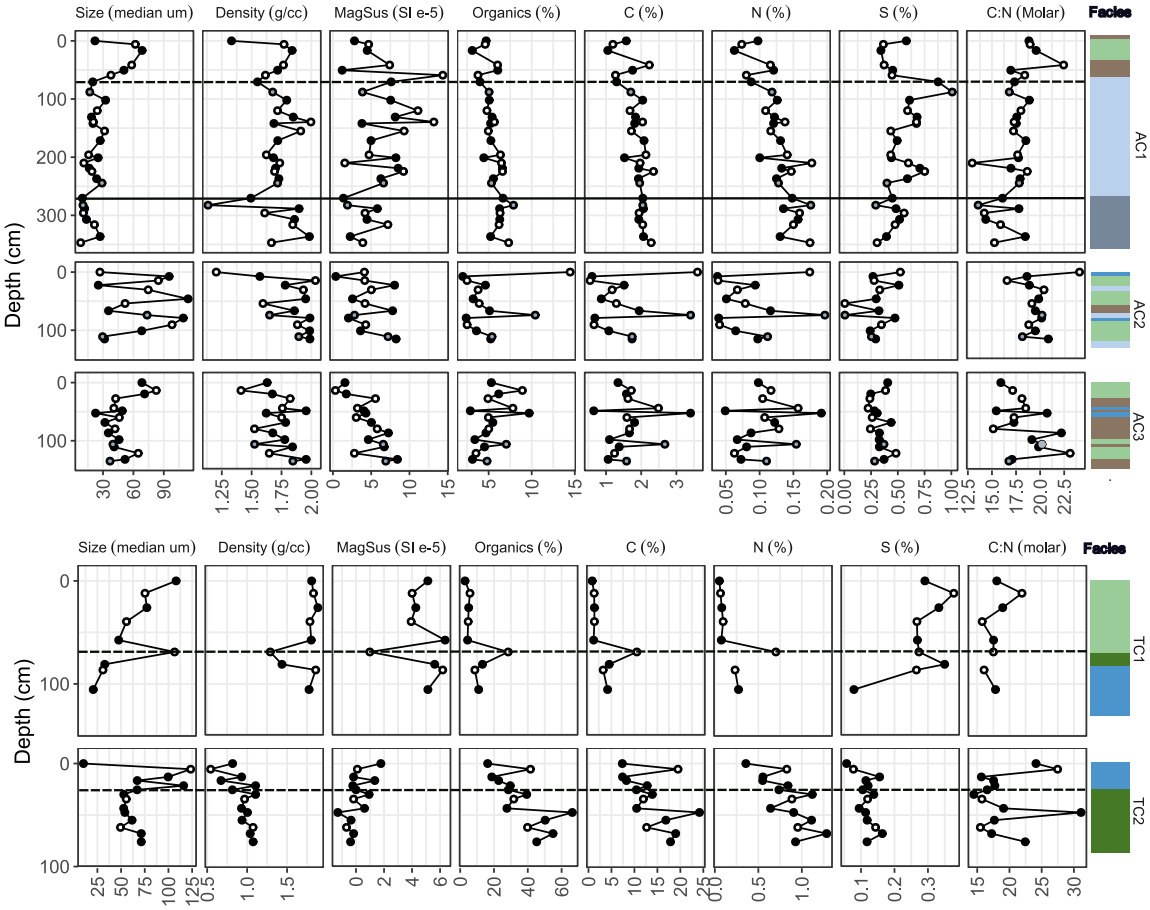

Figure 2.8 Stratigraphic diagrams for alluvial cores AC1, AC2, and AC3, TC1, and TC2. From left to right, parameters are median grain size by percent volume (um), density (g cm^{-3}), magnetic susceptibility (SIe^{-5}), percent mass carbon, percent mass nitrogen, percent mass organics, percent mass sulfur, and the molar ratio between carbon and nitrogen. Facies are denoted by the coloured bars to the right of the stratigraphic parameters, with Facies A (dark blue), Facies B (light green), Facies C (brown), Facies D (light blue), Facies E (dark grey), and Facies F (dark green) represented. White points show samples analyzed for X-ray diffraction (XRD), grey points show samples analyzed for radiocarbon ($\Delta^{14}C$) and XRD, and black points show the remaining samples. The dashed horizontal lines in AC1, TC1, and TC2 mark a transition from high to low energy depostional environment at 70 cm, 69 cm, and 30cm, respectively. The solid horizontal line in AC1 marks the transition from deltaic sediments to lacustrine sediments at 270 cm.

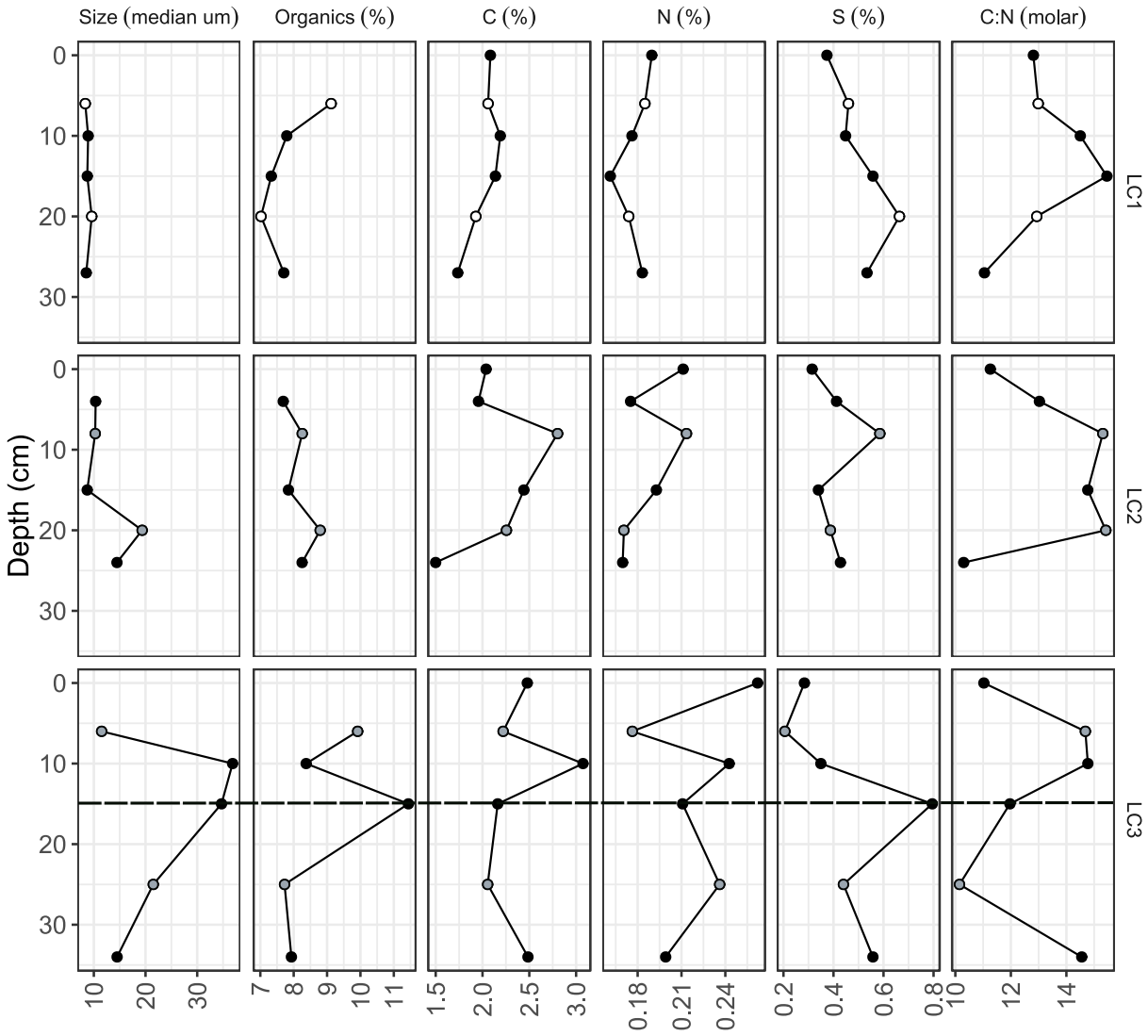

Figure 2.9 Stratigraphic diagrams for gravity cores LC1, LC2, and LC3. From left to right, parameters are median grain size by percent volume (μm), percent mass carbon, percent mass nitrogen, percent mass organics, percent mass sulfur, and the molar ratio between carbon and nitrogen. White points show samples analyzed for X-ray diffraction (XRD), grey points show samples analyzed for radiocarbon ($\Delta^{14}C$) and XRD, and black points show the remaining samples. The dashed horizontal line in LC3 marks the ^{137}Cs peak detected at 15 cm.

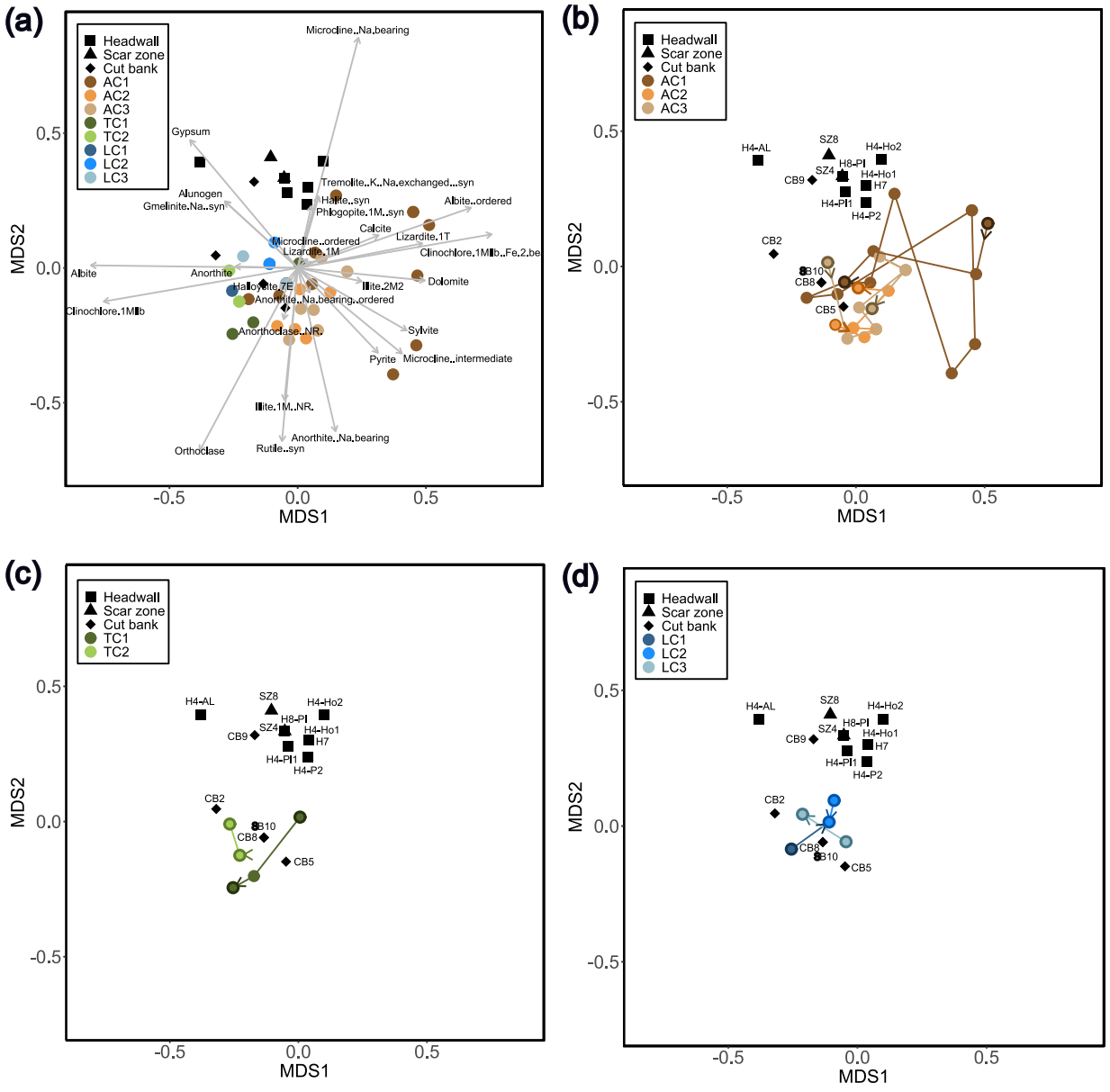

Figure 2.10 NMDS biplots showing X-ray diffraction (XRD) mineralogy (k=2, stress=0.1875). Panel (a) shows all samples analyzed and the mineral vectors. Panel (b) shows the alluvial core samples and the parent materials. Panel (c) shows the terrestrial core samples and the parent materials. Panel (d) shows the lake cores and parent materials. Lines connecting samples in panels (b–d) represent downward movement within each core.

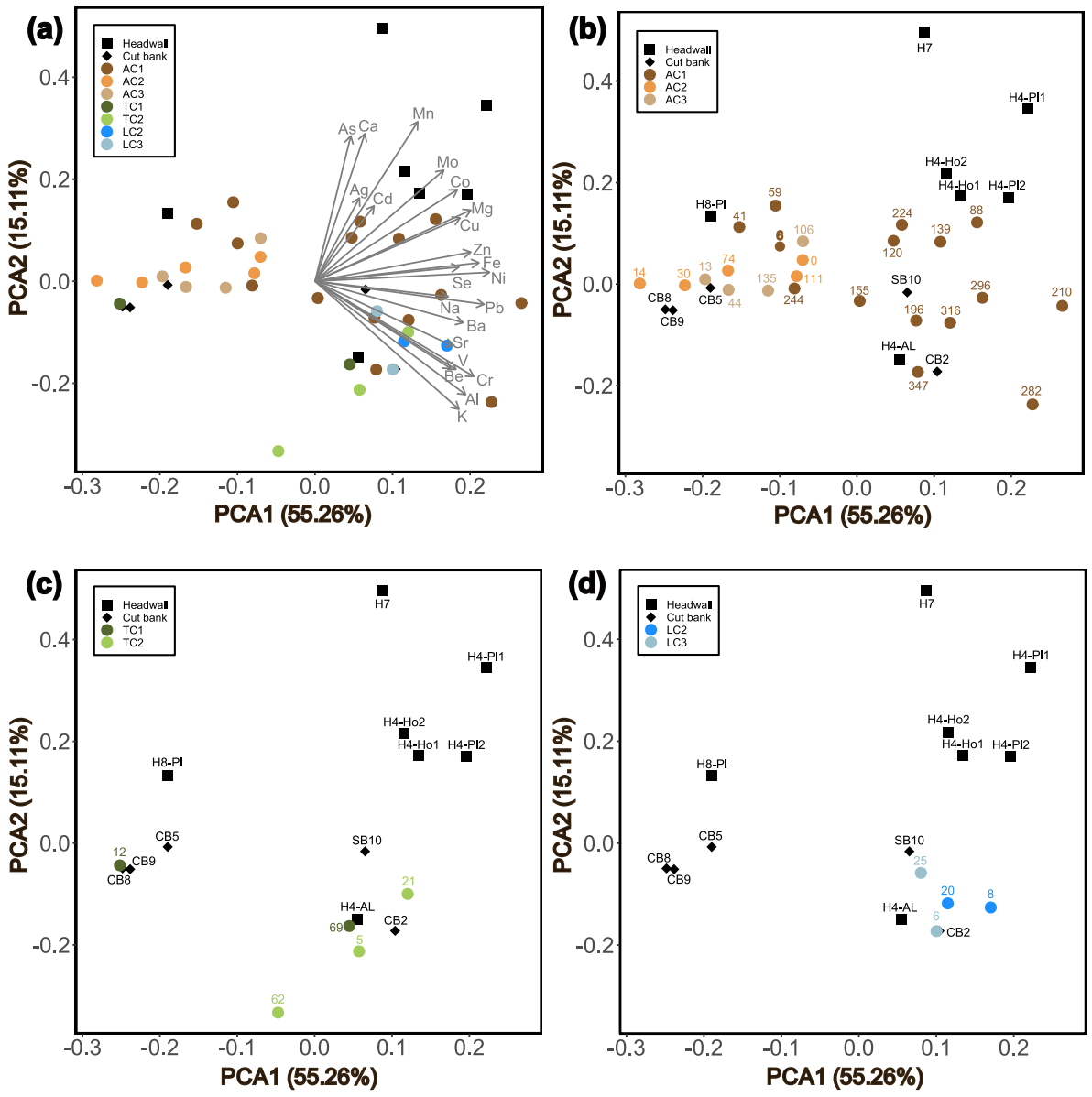

Figure 2.11 Principal Component Analysis (PCA) of cations. Panel (a) shows all samples analyzed and the cation vectors. Panel (b) shows the alluvial core samples and the parent materials. Panel (c) shows the terrestrial core samples and the parent materials. Panel (d) shows the lake cores and parent materials. Depths for alluvial, terrestrial, and lake cores are shown in centimeters by the numerical value adjacent to these points.

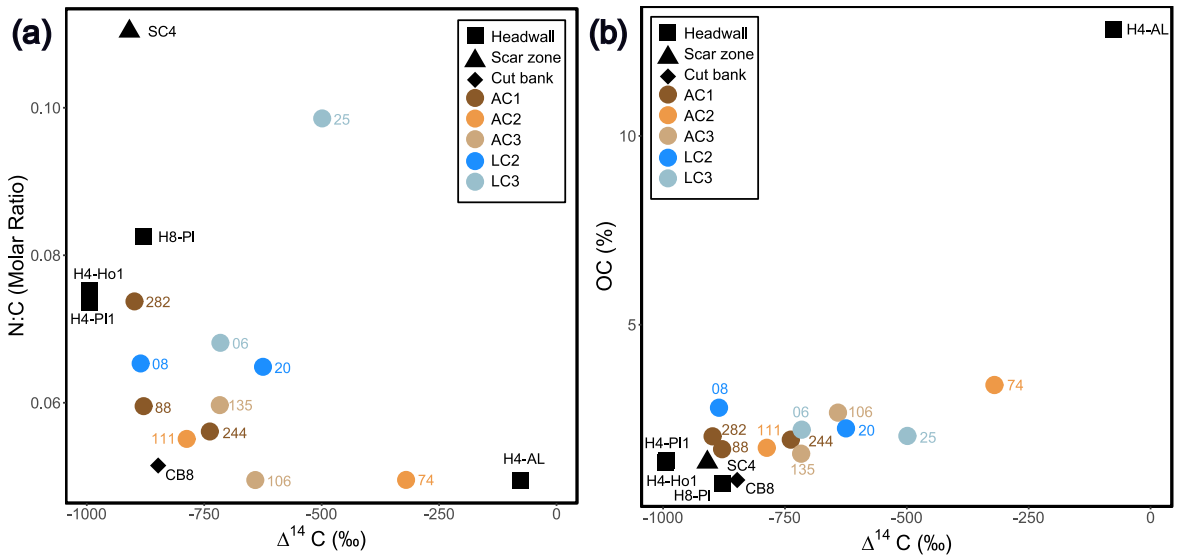

Figure 2.12 Biplots illustrating radiocarbon values. Panel (a) shows $\Delta^{14}C$ (‰) plotted against the molar ratio of nitrogen to carbon. Panel (b) shows $\Delta^{14}C$ (‰) plotted against organic carbon (%) values.

Chapter 3.General conclusion

3.1 Summary of findings

Within the Willow River catchment, thaw-driven mass wasting is accelerating. Since 1986, the number of identified mass wasting features, as well as the size and density of disturbance areas, has accelerated. These changes are likely driven by increasing precipitation in the area, which is accompanied by a shift from a snowfall to rainfall dominated climate (Bintanja & Andry, 2017; Bintanja & Selten, 2014; Kokelj et al., 2015; Lacelle et al., 2015). The number and area of identified debris tongues has also increased since 1986, which is associated with elevated connectivity between terrestrial and aquatic systems. Increasing slope-to-stream connectivity is causing large amounts of permafrost derived materials to be mobilized in fluvial systems (Kokelj, Lantz, et al., 2017; Kokelj, Tunnicliffe, et al., 2017). Not only has this resulted in alterations in fluvial morphology within the Willow River catchment, as witnessed by the rerouting of the main river channel in 2007 (Kokelj et al., 2021), but it has also caused substantial increases in the turbidity of downstream lakes. Another implication of the river reroute is the near-complete infill of Willow Lake, and the formation of a prograding delta within the alluvial surface of the lake. Recently deposited materials within the lake reflect influences from a variety of parent materials, but there has been a shift in the stratigraphic parameters within the lake toward larger grain sizes and lower percentages of organics, organic carbon, and nitrogen, as compared to materials deposited before the river reroute. Not only has accelerated thaw-driven geomorphic change impacted Willow Lake, but there is evidence that a variety of alluvial and downstream aquatic systems are also experiencing permafrost-derived change. These changes emphasize that thaw-induced mass wasting and associated geomorphic change can impact a broad range of environments, the effects of which can propagate across various scales.

3.2 Limitations, improvements, and future directions

In this study, temporal changes in thaw-induced mass wasting were analyzed manually using remote sensing methods. While this was effective, it introduced various limitations including data availability and image resolution, which may have contributed to errors identifying all features. Additionally, the resolution of imagery used (30 m

Landsat) prevented the identification of features that were smaller than captured by pixel resolution. There have been recent efforts to develop remote sensing tools that are able to digitally assess the evolution of thermokarst (Huang et al., 2018; Lara et al., 2019). The use of such products would help to eliminate some of the challenges associated with this component of the project, as well as be much more efficient and allow for the development of high-resolution profiles of temporal change.

We also used remote sensing methods to assess historic trends in lake turbidity, which allowed for relative changes to be assessed between years. While the use of NDTI has been shown to be a good proxy for assessing variation in turbidity (Bid & Siddique, 2019; Garg et al., 2020; Lacaux et al., 2007), the implementation and use of long-term data sets focused on obtaining a suite of physical, chemical, and biological parameters of lakes impacted by thaw-induced mass wasting would be useful when analyzing temporal changes in lakes impacted by thaw-driven mass wasting. This would also help to address limitations in data availability for remote areas such as the Willow River catchment and help to combat any weather-related impacts to image quality and availability.

Although there has been extensive research conducted on thermokarst lakes (Anthony et al., 2014; Korosi et al., 2022; Pokrovsky et al., 2011; Vonk, Tank, Bowden, et al., 2015), and the use of these systems to reconstruct historic conditions (Bouchard et al., 2017), there has been less work focused on assessing the cumulative effects of multiple thermokarst features on impacted lakes (Deison et al., 2012; Kokelj et al., 2005). Lakes are a valuable Arctic resource in terms of ecological function and habitat, as well as for local communities. With recent evidence illustrating that Arctic lake surface area is decreasing (Webb et al., 2022), these systems are clearly at risk from ongoing changes in climate. While lake disappearance via sedimentation, as witnessed within Willow Lake, appears to be uncommon, it is not unheard of in other Arctic areas (Lewkowicz & Way, 2019). Increased efforts to identify similar systems would be rewarded by creating an opportunity to assess the cumulative impacts of thermokarst on downstream systems, help constrain climate predictions, and better prepare local communities for dynamic thaw-induced change.

This study focuses on assessing the composition of fluvially-mobilized sediments and how they change between source and sink regions of a dynamically changing catchment. To build upon the results of this study, it would be valuable to investigate the mass balance relationships occurring within the system to get a sense of the quantity and composition of materials that are moving downstream (Kokelj et al., 2015; van der Sluijs et al., 2018). This would help assess the extent of materials that are being deposited within aquatic and terrestrial environments (Kokelj et al., 2013), as well as provide insight into the proportion of materials that remain suspended and propagate further downstream (Droppo et al., 2022).

A large proportion of permafrost landscapes are primed for climate driven change as temperatures and precipitation continue to rise (Kokelj, Lantz, et al., 2017). Understanding how thaw-driven mass wasting has evolved in the past will help provide the groundwork necessary to predict and respond to future changes in climate. As thermokarst features are becoming more connected to aquatic environments within the Arctic, a larger proportion of terrestrial materials will be liberated to receiving environments. It is important to evaluate the influence of a variety of permafrost-derived materials to assess the effect of increased connectivity on aquatic composition and function. Investigating the fate of permafrost-derived materials will help communities better understand and prepare for local thaw-driven developments that may impact community function, as well as inform decision makers when developing policies to combat and adapt to future changes in climate.

Literature Cited

American Public Health Association, American Water Works Association, & Water Environment Federation. (1999). *Standard Methods for the Examination of Water and Wastewater*.

Anthony, K. M. W., Zimov, S. A., Grosse, G., Jones, M. C., Anthony, P. M., Iii, F. S. C., Finlay, J. C., Mack, M. C., Davydov, S., Frenzel, P., & Frolking, S. (2014). A shift of thermokarst lakes from carbon sources to sinks during the Holocene epoch. *Nature*, *511*(7510), 452–456. https://doi.org/10.1038/nature13560

Ballantyne, C. K. (2002). Paraglacial geomorphology. In *Quaternary Science Reviews* (Vol. 21).

Bates, D., Mächler, M., Bolker, B., & Walker, S. (2015). Fitting Linear Mixed-Effects Models Using lme4. *Journal of Statistical Software*, *67*(1), 1–48. https://doi.org/10.18637/jss.v067.i01

Beel, C. R., Heslop, J. K., Orwin, J. F., Pope, M. A., Schevers, A. J., Hung, J. K. Y., Lafrenière, M. J., & Lamoureux, S. F. (2021). Emerging dominance of summer rainfall driving High Arctic terrestrial-aquatic connectivity. *Nature Communications*, *12*(1). https://doi.org/10.1038/s41467-021-21759-3

Beel, C. R., Lamoureux, S. F., Orwin, J. F., Pope, M. A., Lafrenière, M. J., & Scott, N. A. (2020). Differential impact of thermal and physical permafrost disturbances on High Arctic dissolved and particulate fluvial fluxes. *Scientific Reports*, *10*(1), 11836. https://doi.org/10.1038/s41598-020-68824-3

Bevington, A. E., & Twilley, R. R. (2018). Island Edge Morphodynamics along a Chronosequence in a Prograding Deltaic Floodplain Wetland. *Journal of Coastal Research*, *34*(4), 806–817. https://doi.org/10.2112/JCOASTRES-D-17-00074.1

Bid, S., & Siddique, G. (2019). Identification of seasonal variation of water turbidity using NDTI method in Panchet Hill Dam, India. *Modeling Earth Systems and Environment*, *5*(4), 1179–1200. https://doi.org/10.1007/s40808-019-00609-8

Bintanja, R., & Andry, O. (2017). Towards a rain-dominated Arctic. *Nature Climate Change*, *7*(4), 263–267. https://doi.org/10.1038/nclimate3240

Bintanja, R., & Selten, F. M. (2014). Future increases in Arctic precipitation linked to local evaporation and sea-ice retreat. *Nature*, *509*(7501), 479–482. https://doi.org/10.1038/nature13259

Blaen, P. J., Milner, A. M., Hannah, D. M., Brittain, J. E., & Brown, L. E. (2014). Impact of changing hydrology on nutrient uptake in high arctic rivers. *River Research and Applications*, *30*(9), 1073–1083. https://doi.org/10.1002/rra.2706

Bouchard, F., MacDonald, L. A., Turner, K. W., Thienpont, J. R., Medeiros, A. S., Biskaborn, B. K., Korosi, J., Hall, R. I., Pienitz, R., & Wolfe, B. B. (2017). Paleolimnology of thermokarst lakes: a window into permafrost landscape evolution. *Arctic Science*, *3*(2), 91–117. https://doi.org/10.1139/as-2016-0022

Bowden, W. B., Gooseff, M. N., Balser, A., Green, A., Peterson, B. J., & Bradford, J. (2008). Sediment and nutrient delivery from thermokarst features in the foothills of the North Slope, Alaska: Potential impacts on headwater stream ecosystems. *Journal of Geophysical Research: Biogeosciences*, *113*(2). https://doi.org/10.1029/2007JG000470

Bröder, L., Keskitalo, K., Zolkos, S., Shakil, S., Tank, S. E., Kokelj, S. v., Tesi, T., van Dongen, B. E., Haghipour, N., Eglinton, T. I., & Vonk, J. E. (2021). Preferential export of permafrost-derived organic matter as retrogressive thaw slumping intensifies. *Environmental Research Letters*, *16*(5). https://doi.org/10.1088/1748-9326/abee4b

Burn, C. R. (1997). Cryostratigraphy, paleogeography, and climate change during the early Holocene warm interval, western Arctic coast, Canada. *Canadian Journal of Earth Sciences* , *34*, 912–925. https://doi.org/https://doi.org/10.1139/e17-076

Burn, C. R., & Kokelj, S. v. (2009). The environment and permafrost of the Mackenzie Delta area. *Permafrost and Periglacial Processes*, *20*(2), 83–105. https://doi.org/10.1002/ppp.655

Carson, M. A., Conly, F. M., & Jasper, J. N. (1999). Riverine sediment balance of the Mackenzie Delta, Northwest Territories, Canada. *Hydrological Processes*, *13*(16 SPEC. ISS.), 2499–2518. https://doi.org/10.1002/(SICI)1099-1085(199911)13:16<2499::AID-HYP937>3.0.CO;2-I

Chalov, S., Prokopeva, K., & Habel, M. (2021). North to south variations in the suspended sediment transport budget within large Siberian river deltas revealed by remote sensing data. *Remote Sensing*, *13*(22). https://doi.org/10.3390/rs13224549

Chin, K. S., Lento, J., Culp, J. M., Lacelle, D., & Kokelj, S. v. (2016). Permafrost thaw and intense thermokarst activity decreases abundance of stream benthic macroinvertebrates. *Global Change Biology*, *22*(8), 2715–2728. https://doi.org/10.1111/gcb.13225

Crann, C. A., Murseli, S., St-Jean, G., Zhao, X., Clark, I. D., & Kieser, W. E. (2017). First Status Report on Radiocarbon Sample Preparation Techniques at the A.E. Lalonde AMS Laboratory (Ottawa, Canada). *Radiocarbon*, *59*(3), 695–704. https://doi.org/10.1017/RDC.2016.55

D422-ASTM (1972) Standard test method for particle-size analysis of soils. ASTM International 63:1-8.

Deison, R., Smol, J. P., Kokelj, S. v., Pisaric, M. F. J., Kimpe, L. E., Poulain, A. J., Sanei, H., Thienpont, J. R., & Blais, J. M. (2012). Spatial and temporal assessment of mercury and organic matter in thermokarst affected lakes of the Mackenzie Delta uplands, NT, Canada. *Environmental Science and Technology*, *46*(16), 8748–8755. https://doi.org/10.1021/es300798w

Droppo, I. G., di Cenzo, P., McFadyen, R., & Reid, T. (2022). Assessment of the sediment and associated nutrient/contaminant continuum, from permafrost thaw slump scars to tundra lakes in the western Canadian Arctic. *Permafrost and Periglacial Processes*, *33*(1), 32–45. https://doi.org/10.1002/ppp.2134

Dunnington, D. W., Libera, N., Kurek, J., Spooner, I. S., & Gagnon, G. A. (2022). tidypaleo : Visualizing Paleoenvironmental Archives Using ggplot2. *Journal of Statistical Software*, *101*(7), 1–20. https://doi.org/10.18637/jss.v101.i07

Dyke, A., & Evans, D. (2003). Ice-marginal terrestrial landsystems: Northern Laurentide Ice Sheet margins. In L. Gooster (Ed.), *Glacial landsystems* (pp. 143–165). Routledge. https://doi.org/10.4324/9780203784976

Dyke, A. S., Andrews, J. T., Clark, P. U., England, J. H., Miller, G. H., Shaw, J., & Veillette, J. J. (2002). The Laurentide and Innuitian ice sheets during the Last Glacial Maximum. In *Quaternary Science Reviews* (Vol. 21).

Environment Canada (2022). National climate data and information archive, Inuvik, NWT. https://climate.weather.gc.ca/

Feng, X., Gustafsson, Ö., Holmes, R. M., Vonk, J. E., van Dongen, B. E., Semiletov, I. P., Dudarev, O. v., Yunker, M. B., Macdonald, R. W., Wacker, L., Montluçon, D. B., & Eglinton, T. I. (2015). Multimolecular tracers of terrestrial carbon transfer across the pan-Arctic: 14C characteristics of sedimentary carbon components and their environmental controls. *Global Biogeochemical Cycles*, *29*(11), 1855–1873. https://doi.org/10.1002/2015GB005204

Garg, V., Aggarwal, S. P., & Chauhan, P. (2020). Changes in turbidity along Ganga River using Sentinel-2 satellite data during lockdown associated with COVID-19. *Geomatics, Natural Hazards and Risk*, *11*(1), 1175–1195. https://doi.org/10.1080/19475705.2020.1782482

Gilbert, G. K. (1885). The topographic features of lake shores. In *U.S. Geological Survey 5th Annual Report* (pp. 104–110).

Gilbert, G. K. (1890). Lake Bonneville. In *U.S. Geological Survey Monograph no. 1* (pp. 1–438).

GISTEMP Team. (2022). *GISS Surface Temperature Analysis (GISTEMP), version 4*. NASA Goddard Institute for Space Studies. data.giss.nasa.gov/gistemp/.

Goslee, S. C., & Urban, D. L. (2007). The Ecodist Package for Dissimilarity-based Analysis of Ecological Data. *Journal of Statistical Software*, *22*(7), 1–19. https://doi.org/10.18637/jss.v022.i07

Harris, D., Horwáth, W. R., & van Kessel, C. (2001). Acid fumigation of soils to remove carbonates prior to total organic carbon or carbon-13 isotopic analysis. *Soil Science Society of America Journal*, *65*(6), 1853–1856. https://doi.org/10.2136/sssaj2001.1853

Heiri, O., Lotter, A. F., & Lemcke, G. (2001). Loss on ignition as a method for estimating organic and carbonate content in sediments: reproducibility and comparability of results. . *Journal of Paleolimnology*, *25*(1), 101–110. https://doi.org/10.1023/A:1008119611481

Horikoshi, M., & Tang, Y. (2018). *ggfortify: Data Visualization Tools for Statistical Analysis Results*. https://CRAN.R-project.org/package=ggfortify

Huang, L., Liu, L., Jiang, L., & Zhang, T. (2018). Automatic mapping of thermokarst landforms from remote sensing images using deep learning: A case study in the northeastern Tibetan Plateau. *Remote Sensing*, *10*(12). https://doi.org/10.3390/rs10122067

IPCC. (2014). *Climate change 2014 : synthesis report* (Core Writing Team, R. K. Pachauri, & L. A. Meyer, Eds.). Contribution of Working Groups I, II and III to the Fifth Assessment Report of the Intergovernmental Panel on Climate Change.

Jones, B. M., Grosse, G., Farquharson, L. M., Roy-Léveillée, P., Veremeeva, A., Kanevskiy, M. Z., Gaglioti, B. v., Breen, A. L., Parsekian, A. D., Ulrich, M., & Hinkel, K. M. (2022). Lake and drained lake basin systems in lowland permafrost regions. *Nature Reviews Earth & Environment*, *3*(1), 85–98. https://doi.org/10.1038/s43017-021-00238-9

Kokelj, S. V., & Burn, C. R. (2005). Geochemistry of the active layer and near-surface permafrost, Mackenzie delta region, Northwest Territories, Canada. *Canadian Journal of Earth Sciences*, *42*(1), 37–48. https://doi.org/10.1139/E04-089

Kokelj, S. V., Jenkins, R. E., Milburn, D., Burn, C. R., & Snow, N. (2005). The influence of thermokarst disturbance on the water quality of small upland lakes, Mackenzie Delta region, Northwest Territories, Canada. *Permafrost and Periglacial Processes*, *16*(4), 343–353. https://doi.org/10.1002/ppp.536

Kokelj, S. V, & Jorgenson, M. T. (2013). Advances in thermokarst research. *Permafrost and Periglacial Processes*, *24*(2), 108–119. https://doi.org/10.1002/ppp.1779

Kokelj, S. V., Kokoszka, J., van der Sluijs, J., Rudy, A. C. A., Tunnicliffe, J., Shakil, S., Tank, S. E., & Zolkos, S. (2021). Thaw-driven mass wasting couples slopes with downstream systems, and effects propagate through Arctic drainage networks. *Cryosphere*, *15*(7), 3059–3081. https://doi.org/10.5194/tc-15-3059-2021

Kokelj, S. V., Lacelle, D., Lantz, T. C., Tunnicliffe, J., Malone, L., Clark, I. D., & Chin, K. S. (2013). Thawing of massive ground ice in mega slumps drives increases in stream sediment and solute flux across a range of watershed scales. *Journal of Geophysical Research: Earth Surface*, *118*(2), 681–692. https://doi.org/10.1002/jgrf.20063

Kokelj, S. V., Lantz, T. C., Kanigan, J., Smith, S. L., & Coutts, R. (2009). Origin and polycyclic behaviour of tundra thaw slumps, Mackenzie Delta region, Northwest Territories, Canada. *Permafrost and Periglacial Processes*, *20*(2), 173–184. https://doi.org/10.1002/ppp.642

Kokelj, S. V., Lantz, T. C., Tunnicliffe, J., Segal, R., & Lacelle, D. (2017). Climate-driven thaw of permafrost preserved glacial landscapes, northwestern Canada. *Geology*, *45*(4), 371–374. https://doi.org/10.1130/G38626.1

Kokelj, S. V., Tunnicliffe, J. F., & Lacelle, D. (2017). The Peel Plateau of Northwestern Canada: An Ice-Rich Hummocky Moraine Landscape in Transition. In *In: Slaymaker, O. (eds) Landscapes and Landforms of Western Canada. World Geomorphological Landscapes.* (pp. 109–122). https://doi.org/10.1007/978-3-319-44595-3_7

Kokelj, S. V., Tunnicliffe, J., Lacelle, D., Lantz, T. C., Chin, K. S., & Fraser, R. (2015). Increased precipitation drives mega slump development and destabilization of ice-rich permafrost terrain, northwestern Canada. *Global and Planetary Change*, *129*, 56–68. https://doi.org/10.1016/j.gloplacha.2015.02.008

Kokelj, S. V., Zajdlik, B., & Thompson, M. S. (2009). The impacts of Thawing permafrost on the chemistry of lakes across the subarctic boreal-tundra transition, Mackenzie Delta region, Canada. *Permafrost and Periglacial Processes*, *20*(2), 185–199. https://doi.org/10.1002/ppp.641

Korosi, J. B., Coleman, K. A., Hoskin, G. N., Little, A. J., Stewart, E. M., & Thienpont, J. R. (2022). Paleolimnological perspectives on the shifting geographic template of permafrost landscapes and its implications for Arctic freshwater biodiversity. *Canadian Journal of Fisheries and Aquatic Sciences*, *79*(7), 1162–1172. https://doi.org/10.1139/cjfas-2021-0280

Kostic, S., & Parker, G. (2003). Progradational sand-mud deltas in lakes and reservoirs. Part 2. Experiment and numerical simulation. *Journal of Hydraulic Research*, *41*(2), 141–152. https://doi.org/10.1080/00221680309499957

Lacaux, J. P., Tourre, Y. M., Vignolles, C., Ndione, J. A., & Lafaye, M. (2007). Classification of ponds from high-spatial resolution remote sensing: Application to Rift Valley Fever epidemics in Senegal. *Remote Sensing of Environment*, *106*(1), 66–74. https://doi.org/10.1016/j.rse.2006.07.012

Lacelle, D., Bjornson, J., & Lauriol, B. (2010). Climatic and geomorphic factors affecting contemporary (1950-2004) activity of retrogressive thaw slumps on the Aklavik plateau, Richardson mountains, NWT, Canada. *Permafrost and Periglacial Processes*, *21*(1), 1–15. https://doi.org/10.1002/ppp.666

Lacelle, D., Bjornson, J., Lauriol, B., Clark, I. D., & Troutet, Y. (2004). Segregated-intrusive ice of subglacial meltwater origin in retrogressive thaw flow headwalls, Richardson Mountains, NWT, Canada. *Quaternary Science Reviews*, *23*(5–6), 681–696. https://doi.org/10.1016/j.quascirev.2003.09.005

Lacelle, D., Brooker, A., Fraser, R. H., & Kokelj, S. V. (2015). Distribution and growth of thaw slumps in the Richardson Mountains–Peel Plateau region, northwestern Canada. *Geomorphology*, *235*, 40–51. https://doi.org/10.1016/j.geomorph.2015.01.024

Lacelle, D., Lauriol, B., Zazula, G., Ghaleb, B., Utting, N., & Clark, I. D. (2013). Timing of advance and basal condition of the Laurentide Ice Sheet during the last glacial maximum in the Richardson Mountains, NWT. *Quaternary Research*, *80*(2), 274–283. https://doi.org/10.1016/j.yqres.2013.06.001

Lantuit, H., & Pollard, W. H. (2008). Fifty years of coastal erosion and retrogressive thaw slump activity on Herschel Island, southern Beaufort Sea, Yukon Territory, Canada. *Geomorphology*, *95*(1–2), 84–102. https://doi.org/10.1016/j.geomorph.2006.07.040

Lara, M. J., Chipman, M. L., & Hu, F. S. (2019). Automated detection of thermoerosion in permafrost ecosystems using temporally dense Landsat image stacks. *Remote Sensing of Environment*, *221*, 462–473. https://doi.org/10.1016/j.rse.2018.11.034

Lattaud, J., Bröder, L., Haghipour, N., Rickli, J., Giosan, L., & Eglinton, T. I. (2021). Influence of Hydraulic Connectivity on Carbon Burial Efficiency in Mackenzie Delta Lake Sediments. *Journal of Geophysical Research: Biogeosciences*, *126*(3). https://doi.org/10.1029/2020JG006054

Lenssen, N. J. L., Schmidt, G. A., Hansen, J. E., Menne, M. J., Persin, A., Ruedy, R., & Zyss, D. (2019). Improvements in the GISTEMP Uncertainty Model. *Journal of Geophysical Research: Atmospheres*, *124*(12), 6307–6326. https://doi.org/10.1029/2018JD029522

Lewkowicz, A. G., & Way, R. G. (2019). Extremes of summer climate trigger thousands of thermokarst landslides in a High Arctic environment. *Nature Communications*, *10*(1). https://doi.org/10.1038/s41467-019-09314-7

Mahony, C. R., Wang, T., Hamann, A., & Cannon, A. J. (2022). A global climate model ensemble for downscaled monthly climate normals over North America. *International Journal of Climatology*, *42*(11), 5871–5891. https://doi.org/10.1002/joc.7566

Malone, L., Lacelle, D., Kokelj, S., & Clark, I. D. (2013). Impacts of hillslope thaw slumps on the geochemistry of permafrost catchments (Stony Creek watershed, NWT, Canada). *Chemical Geology*, *356*, 38–49. https://doi.org/10.1016/j.chemgeo.2013.07.010

Marsh, P., & Hey, M. (1989). The Flooding Hydrology of Mackenzie Delta Lakes near Inuvik, N.W.T., Canada. *Arctic*, *42*(1), 41–49.

Marsh, P., & Hey, M. (1994). Analysis of Spring High Water Events in the Mackenzie Delta and Implications for Lake and Terrestrial Flooding. *Geografiska Annaler: Series A, Physical Geography*, *76*(4), 221–234. https://doi.org/10.1080/04353676.1994.11880420

Mather, A. E., Stokes, M., & Whitfield, E. (2017). River terraces and alluvial fans: The case for an integrated Quaternary fluvial archive. *Quaternary Science Reviews*, *166*, 74–90. https://doi.org/10.1016/j.quascirev.2016.09.022

Mesquita, P. S., Wrona, F. J., & Prowse, T. D. (2010). Effects of retrogressive permafrost thaw slumping on sediment chemistry and submerged macrophytes in Arctic tundra lakes. *Freshwater Biology*, *55*(11), 2347–2358. https://doi.org/10.1111/j.1365-2427.2010.02450.x

Michelutti, N., Hay, M. B., Marsh, P., Lesack, L., & Smol, J. P. (2001). Diatom Changes in Lake Sediments from the Mackenzie Delta, N.W.T., Canada: Paleohydrological Applications. *Arctic, Antarctic, and Alpine Research*, *33*(1), 1–12. https://doi.org/10.1080/15230430.2001.12003398

Muggeo, V. M. R. (2003). Estimating regression models with unknown break-points. *Statistics in Medicine*, *22*, 3055–3071.

Muggeo, V. M. R. (2008). segmented: an R Package to Fit Regression Models with Broken-Line Relationships. *R News*, *8*(1), 20–25. https://cran.r-project.org/doc/Rnews/

Murdoch, A., Gray, D. K., Korosi, J., Vucic, J. M., Cohen, R. S., & Sharma, S. (2021). Drivers of fish biodiversity in a rapidly changing permafrost landscape. *Freshwater Biology*, *66*(12), 2301–2321. https://doi.org/10.1111/fwb.13834

Murseli, S., Middlestead, P., St-Jean, G., Zhao, X., Jean, C., Crann, C. A., Kieser, W. E., & Clark, I. D. (2019). The Preparation of Water (DIC, DOC) and Gas (CO_2, CH_4) Samples for Radiocarbon Analysis at AEL-AMS, Ottawa, Canada. *Radiocarbon*, *61*(5), 1563–1571. https://doi.org/10.1017/RDC.2019.14

Murton, J. B., & French, H. M. (1994). Cryostructures in permafrost, Tuktoyaktuk coastlands, western arctic Canada. In *J. Earth Sci* (Vol. 31).

Overland, J. E., Wang, M., Walsh, J. E., Christensen, J. H., Kattsov, V. M., & Chapman, W. L. (2011). 3. Climate Model Projections for the Arctic. In *Snow, Water, Ice,and Permafrost in the Arctic (SWIPA)*.

Perdue, E. M., & Koprivnjak, J. F. (2007). Using the C/N ratio to estimate terrigenous inputs of organic matter to aquatic environments. *Estuarine, Coastal and Shelf Science*, *73*(1–2), 65–72. https://doi.org/10.1016/j.ecss.2006.12.021

Pokrovsky, O. S., Shirokova, L. S., Kirpotin, S. N., Audry, S., Viers, J., & Dupré, B. (2011). Effect of permafrost thawing on organic carbon and trace element colloidal speciation in the thermokarst lakes of western Siberia. *Biogeosciences*, *8*(3), 565–583. https://doi.org/10.5194/bg-8-565-2011

R Core Team. (2022). *R: A Language and Environment for Statistical Computing*. R Foundation for Statistical Computing. URL https://www.R-project.org/

Ramnarine, R., Voroney, R. P., Wagner-Riddle, C., & Dunfield, K. E. (2011). Carbonate removal by acid fumigation for measuring the $\delta^{13}C$ of soil organic carbon. *Canadian Journal of Soil Science*, *91*(2), 247–250. https://doi.org/10.4141/cjss10066

Rawlins, M. A., Steele, M., Holland, M. M., Adam, J. C., Cherry, J. E., Francis, J. A., Groisman, P. Y., Hinzman, L. D., Huntington, T. G., Kane, D. L., Kimball, J. S., Kwok, R., Lammers, R. B., Lee, C. M., Lettenmaier, D. P., Mcdonald, K. C., Podest, E., Pundsack, J. W., Rudels, B., … Zhang, T. (2010). Analysis of the Arctic system for freshwater cycle intensification: Observations and expectations. *Journal of Climate*, *23*(21), 5715–5737. https://doi.org/10.1175/2010JCLI3421.1

Roberts, K. E., Lamoureux, S. F., Kyser, T. K., Muir, D. C. G., Lafrenière, M. J., Iqaluk, D., Pieńkowski, A. J., & Normandeau, A. (2017). Climate and permafrost effects on the chemistry and ecosystems of High Arctic Lakes. *Scientific Reports*, *7*(1). https://doi.org/10.1038/s41598-017-13658-9

Romanovsky, V. E., Smith, S. L., & Christiansen, H. H. (2010). Permafrost thermal state in the polar northern hemisphere during the international polar year 2007-2009: A synthesis. *Permafrost and Periglacial Processes*, *21*(2), 106–116. https://doi.org/10.1002/ppp.689

Schelske, C. L., Peplow, A., Brenner, M., & Spencer, C. N. (1994). Low-background gamma counting: applications for ^{210}Pb dating of sediments. *Journal of Paleolimnology*, *10*(2), 115–128. https://doi.org/10.1007/BF00682508

Schuur, E. A. G., & Mack, M. C. (2018). *Ecological Response to Permafrost Thaw and Consequences for Local and Global Ecosystem Services*. https://doi.org/10.1146/annurev-ecolsys-121415

Schuur, E. A. G., McGuire, A. D., Schädel, C., Grosse, G., Harden, J. W., Hayes, D. J., Hugelius, G., Koven, C. D., Kuhry, P., Lawrence, D. M., Natali, S. M., Olefeldt, D., Romanovsky, V. E., Schaefer, K., Turetsky, M. R., Treat, C. C., & Vonk, J. E.

(2015). Climate change and the permafrost carbon feedback. *Nature*, *520*(7546), 171–179. https://doi.org/10.1038/nature14338

Segal, R. A., Lantz, T. C., & Kokelj, S. V. (2016). Acceleration of thaw slump activity in glaciated landscapes of the Western Canadian Arctic. *Environmental Research Letters*, *11*(3), 0. https://doi.org/10.1088/1748-9326/11/3/034025

Shakil, S., Tank, S. E., Kokelj, S. V., Vonk, J. E., & Zolkos, S. (2020). Particulate dominance of organic carbon mobilization from thaw slumps on the Peel Plateau, NT: Quantification and implications for stream systems and permafrost carbon release. *Environmental Research Letters*. https://doi.org/10.1088/1748-9326/abac36

Shakil, S., Tank, S. E., Vonk, J. E., & Zolkos, S. (2022). Low biodegradability of particulate organic carbon mobilized from thaw slumps on the Peel Plateau, NT, and possible chemosynthesis and sorption effects. *Biogeosciences*, *19*(7), 1871–1890. https://doi.org/10.5194/bg-19-1871-2022

Shields, M. R., Bianchi, T. S., Kolker, A. S., Kenney, W. F., Mohrig, D., Osborne, T. Z., & Curtis, J. H. (2019). Factors Controlling Storage, Sources, and Diagenetic State of Organic Carbon in a Prograding Subaerial Delta: Wax Lake Delta, Louisiana. *Journal of Geophysical Research: Biogeosciences*, *124*(5), 1115–1131. https://doi.org/10.1029/2018JG004683

Smith, S. L., Burgess, M. M., Riseborough, D., & Nixon, F. M. (2005). Recent trends from Canadian permafrost thermal monitoring network sites. *Permafrost and Periglacial Processes*, *16*(1), 19–30. https://doi.org/10.1002/ppp.511

Stuiver, M., & Polach, H. (1977). Discussion: Reporting of ^{14}C Data. *Radiocarbon*, *19*, 355–363.

Tang, Y., Horikoshi, M., & Li, W. (2016). ggfortify: Unified Interface to Visualize Statistical Result of Popular R Packages. *The R Journal*, *8*(2), 474–485. https://doi.org/10.32614/RJ-2016-060

Tank, S. E., Vonk, J. E., Walvoord, M. A., McClelland, J. W., Laurion, I., & Abbott, B. W. (2020). Landscape matters: Predicting the biogeochemical effects of permafrost thaw on aquatic networks with a state factor approach. *Permafrost and Periglacial Processes*, *31*(3), 358–370. https://doi.org/10.1002/ppp.2057

Thompson, M. S., Wrona, F. J., & Prowse, T. D. (2012). Shifts in Plankton, Nutrient and Light Relationships in Small Tundra Lakes Caused by Localized Permafrost Thaw. *Arctic* , *20*, 367–376. https://doi.org/10.14430/arctic4235.

Turetsky, M. R., Abbott, B. W., Jones, M. C., Anthony, K. W., Olefeldt, D., Schuur, E. A. G., Grosse, G., Kuhry, P., Hugelius, G., Koven, C., Lawrence, D. M., Gibson, C., Sannel, A. B. K., & McGuire, A. D. (2020). Carbon release through abrupt

permafrost thaw. *Nature Geoscience*, *13*(2), 138–143. https://doi.org/10.1038/s41561-019-0526-0

van der Sluijs, J., Kokelj, S. V., Fraser, R. H., Tunnicliffe, J., & Lacelle, D. (2018). Permafrost terrain dynamics and infrastructure impacts revealed by UAV photogrammetry and thermal imaging. *Remote Sensing*, *10*(11). https://doi.org/10.3390/rs10111734

Vonk, J. E., Tank, S. E., Bowden, W. B., Laurion, I., Vincent, W. F., Alekseychik, P., Amyot, M., Billet, M. F., Canário, J., Cory, R. M., Deshpande, B. N., Helbig, M., Jammet, M., Karlsson, J., Larouche, J., MacMillan, G., Rautio, M., Walter Anthony, K. M., & Wickland, K. P. (2015). Reviews and syntheses: Effects of permafrost thaw on Arctic aquatic ecosystems. *Biogeosciences*, *12*(23), 7129–7167. https://doi.org/10.5194/bg-12-7129-2015

Vonk, J. E., Tank, S. E., Mann, P. J., Spencer, R. G. M., Treat, C. C., Striegl, R. G., Abbott, B. W., & Wickland, K. P. (2015). Biodegradability of dissolved organic carbon in permafrost soils and aquatic systems: A meta-analysis. *Biogeosciences*, *12*(23), 6915–6930. https://doi.org/10.5194/bg-12-6915-2015

Vucic, J. M., Gray, D. K., Cohen, R. S., Syed, M., Murdoch, A. D., & Sharma, S. (2020). Changes in water quality related to permafrost thaw may significantly impact zooplankton in small Arctic lakes. *Ecological Applications*, *30*(8). https://doi.org/10.1002/eap.2186

Wacker, L., Bonani, G., Friedrich, M., Hajdas, I., Kromer, B., Němec, M., Ruff, M., Suter, M., Synal, H.-A., & Vockenhuber, C. (2010). MICADAS: Routine and High-Precision Radiocarbon Dating. *Radiocarbon*, *52*(2), 252–262. https://doi.org/10.1017/S0033822200045288

Walter E. Dean, Jr. (1974). Determination of Carbonate and Organic Matter in Calcareous Sediments and Sedimentary Rocks by Loss on Ignition: Comparison With Other Methods. *SEPM Journal of Sedimentary Research*, *Vol. 44*. https://doi.org/10.1306/74D729D2-2B21-11D7-8648000102C1865D

Walthert, L., Graf, U., Kammer, A., Luster, J., Pezzotta, D., Zimmermann, S., & Hagedorn, F. (2010). Determination of organic and inorganic carbon, $\delta^{13}C$, and nitrogen in soils containing carbonates after acid fumigation with HCl. *Journal of Plant Nutrition and Soil Science*, *173*(2), 207–216. https://doi.org/10.1002/jpln.200900158

Wang, T., Hamann, A., Spittlehouse, D., & Carroll, C. (2016). Locally Downscaled and Spatially Customizable Climate Data for Historical and Future Periods for North America. *PLOS ONE*, *11*(6), e0156720. https://doi.org/10.1371/journal.pone.0156720

Webb, E. E., Liljedahl, A. K., Cordeiro, J. A., Loranty, M. M., Witharana, C., & Lichstein, J. W. (2022). Permafrost thaw drives surface water decline across lake-rich regions of the Arctic. *Nature Climate Change*, *12*(9), 841–846. https://doi.org/10.1038/s41558-022-01455-w

Whiteside, J. H., Olsen, P. E., Eglinton, T. I., Cornet, B., McDonald, N. G., & Huber, P. (2011). Pangean great lake paleoecology on the cusp of the end-Triassic extinction. *Palaeogeography, Palaeoclimatology, Palaeoecology*, *301*(1–4), 1–17. https://doi.org/10.1016/j.palaeo.2010.11.025

Wickham, H. (2007). Reshaping data with the reshape package. *Journal of Statistical Software*, *21*(12). https://www.jstatsoft.org/v21/i12/

Wickham, H. (2016). *ggplot2: Elegant Graphics for Data Analysis*. Springer-Verlag New York. https://ggplot2.tidyverse.org

Wickham, H. (2019). *stringr: Simple, Consistent Wrappers for Common String Operations* (R package version 1.4.0). https://CRAN.R-project.org/package=stringr

Wickham, H., Averick, M., Bryan, J., Chang, W., McGowan, L., François, R., Grolemund, G., Hayes, A., Henry, L., Hester, J., Kuhn, M., Pedersen, T., Miller, E., Bache, S., Müller, K., Ooms, J., Robinson, D., Seidel, D., Spinu, V., … Yutani, H. (2019). Welcome to the Tidyverse. *Journal of Open Source Software*, *4*(43), 1686. https://doi.org/10.21105/joss.01686

Yu, L., & Zhong, S. (2021). Trends in Arctic seasonal and extreme precipitation in recent decades. *Theoretical and Applied Climatology*, *145*(3–4), 1541–1559. https://doi.org/10.1007/s00704-021-03717-7

Zolkos, S., & Tank, S. E. (2020). Experimental Evidence That Permafrost Thaw History and Mineral Composition Shape Abiotic Carbon Cycling in Thermokarst-Affected Stream Networks. *Frontiers in Earth Science*, *8*. https://doi.org/10.3389/feart.2020.00152

Zolkos, S., Tank, S. E., & Kokelj, S. V. (2018). Mineral Weathering and the Permafrost Carbon-Climate Feedback. *Geophysical Research Letters*, *45*(18), 9623–9632. https://doi.org/10.1029/2018GL078748

Appendix 1. Supporting Information for Chapter 2

Table A1. Sample descriptions.

Sample ID	Location	Sample Type	Borehole depth	Collection period
AC1	Willow Lake, near shore	CRREL Core	327 cm	Spring 2021
AC1	Willow Lake, middle	CRREL Core	160 cm	Spring 2021
AC3	Willow Lake, near channel	CRREL Core	152 cm	Spring 2021
TC1	Willow River, cut bank	CRREL Core	120 cm	Spring 2021
TC2	Willow Lake, shore	CRREL Core	105 cm	Spring 2021
LC1	Delta lake, near Willow Lake	Gravity core	28 cm	Spring 2021
LC2	Delta Lake, middle	Gravity core	24 cm	Spring 2021
LC3	Delta lake, far	Gravity core	35 cm	Spring 2021
H4-AL	Retrogressive thaw slump (WR-E1), active layer	Bulk sediment	*N/A*	Spring 2021
H4-Ho1	Retrogressive thaw slump (WR-E1), Holocene layer	3” diamond tooth core	*N/A*	Spring 2021
H4-Ho2	Retrogressive thaw slump (WR-E1), Holocene layer	3” diamond tooth core	*N/A*	Spring 2021
H4-Pl1	Retrogressive thaw slump (WR-E1), Pleistocene layer	3” diamond tooth core	*N/A*	Spring 2021
H4-Pl2	Retrogressive thaw slump (WR-E1), Pleistocene layer	3” diamond tooth core	*N/A*	Spring 2021
SZ4	Retrogressive thaw slump (WR-E1), scar zone	Bulk sediment	*N/A*	Summer 2021
H7	Landslide feature, scree	Bulk sediment	*N/A*	Summer 2021
H8-Pl	Retrogressive thaw slump (WR-E5), headwall sample	Bulk sediment	*N/A*	Summer 2021
SZ8	Retrogressive thaw slump (WR-E5), scar zone	Bulk sediment	*N/A*	Summer 2021
CB2	Willow River cutbank, transect site WR-W1	Bulk sediment	*N/A*	Summer 2021
CB5	Willow River cutbank, transect site WR-W2, downstream WR-E1	Bulk sediment	*N/A*	Summer 2021
CB8	Willow River cutbank, transect site WR-W5, downstream WR-E5	Bulk sediment	*N/A*	Summer 2021
CB9	Willow River cutbank, transect site WR-W6, upstream Willow Lake	Bulk sediment	*N/A*	Summer 2021
SB10	Willow River stream bed, transect site WR-W7, downstream Willow Lake	Bulk sediment	*N/A*	Summer 2021

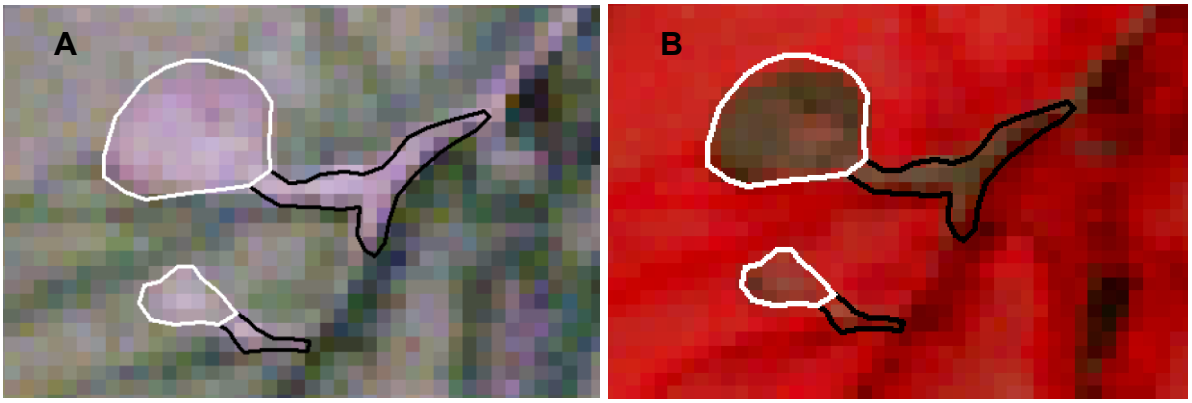

Figure A1. A true colour (A) and false colour (B) image depicting the classification of scar zone (white) and debris tongue (black) delineation.

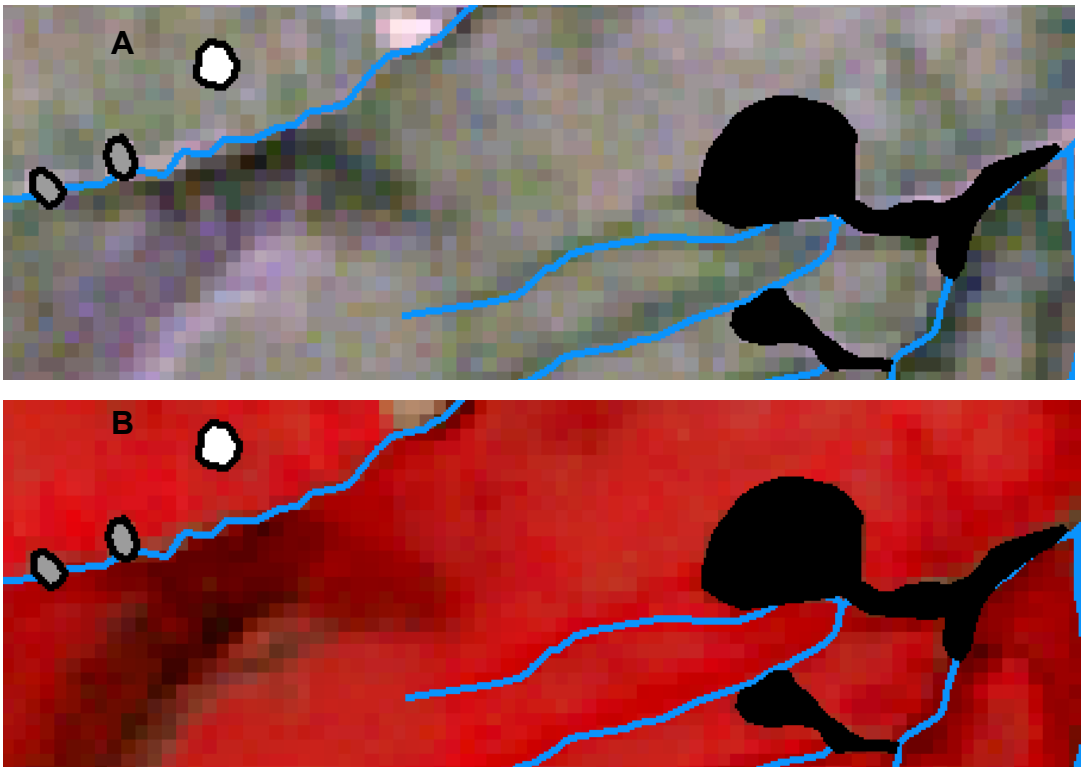

Figure A2. A true colour (A) and false colour (B) image depicting the classification of feature connectivity to the aquatic system. Connectivity of 0 is depicted in white, 1 is displayed as grey, and 2 is shown in black.

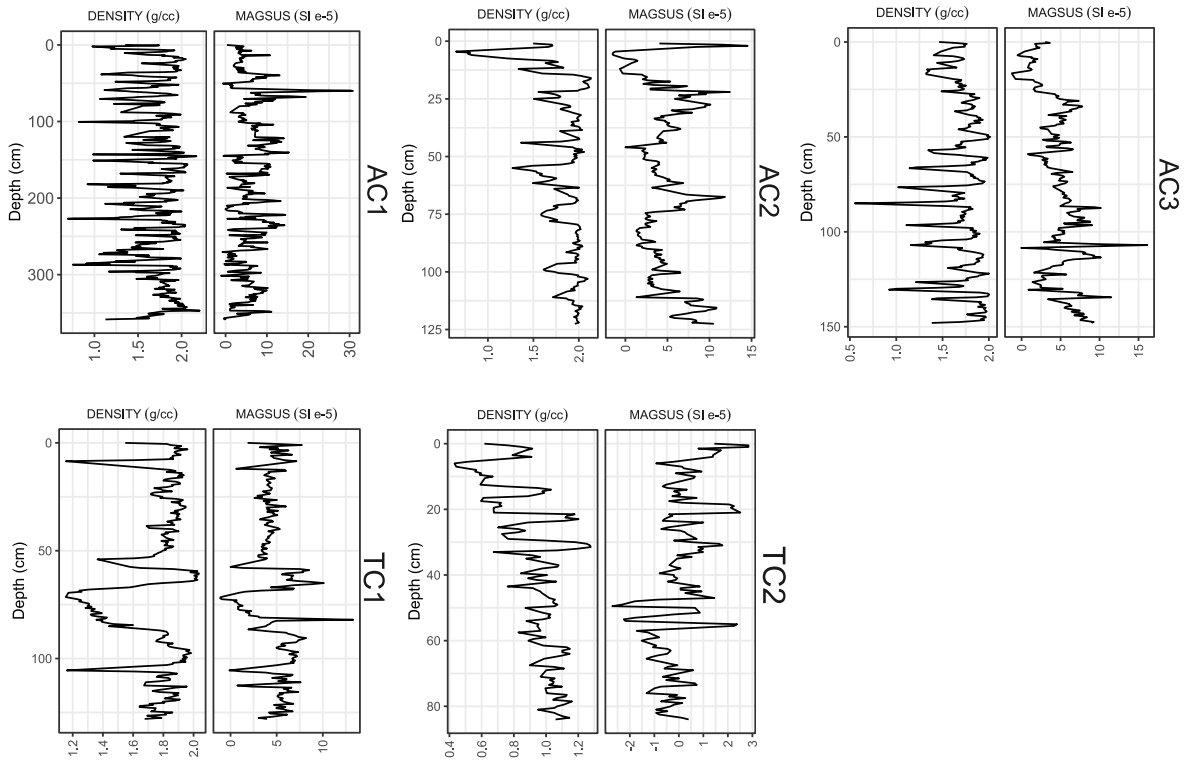

Figure A3. High resolution stratigraphic diagrams of density (g cm^{-3}) and magnetic susceptibility (SIe^{-5}) for alluvial and terrestrial cores.

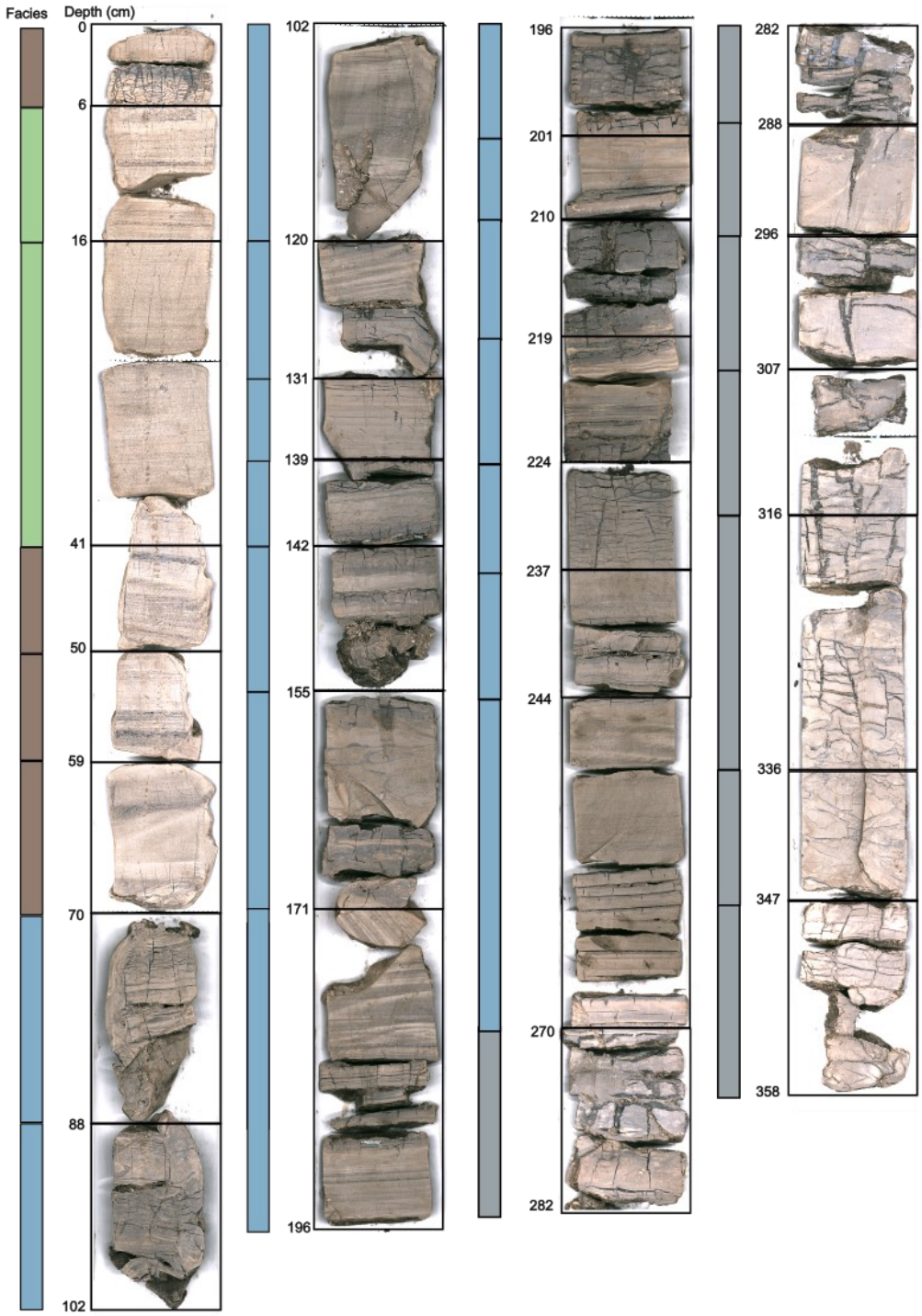

Figure A4. Ultra high-resolution images for alluvial core 1 (AC1). Facies B is represented by the light green, Facies C is represented by the brown, Facies D is represented by the light blue, and Facies E is represented by the grey.

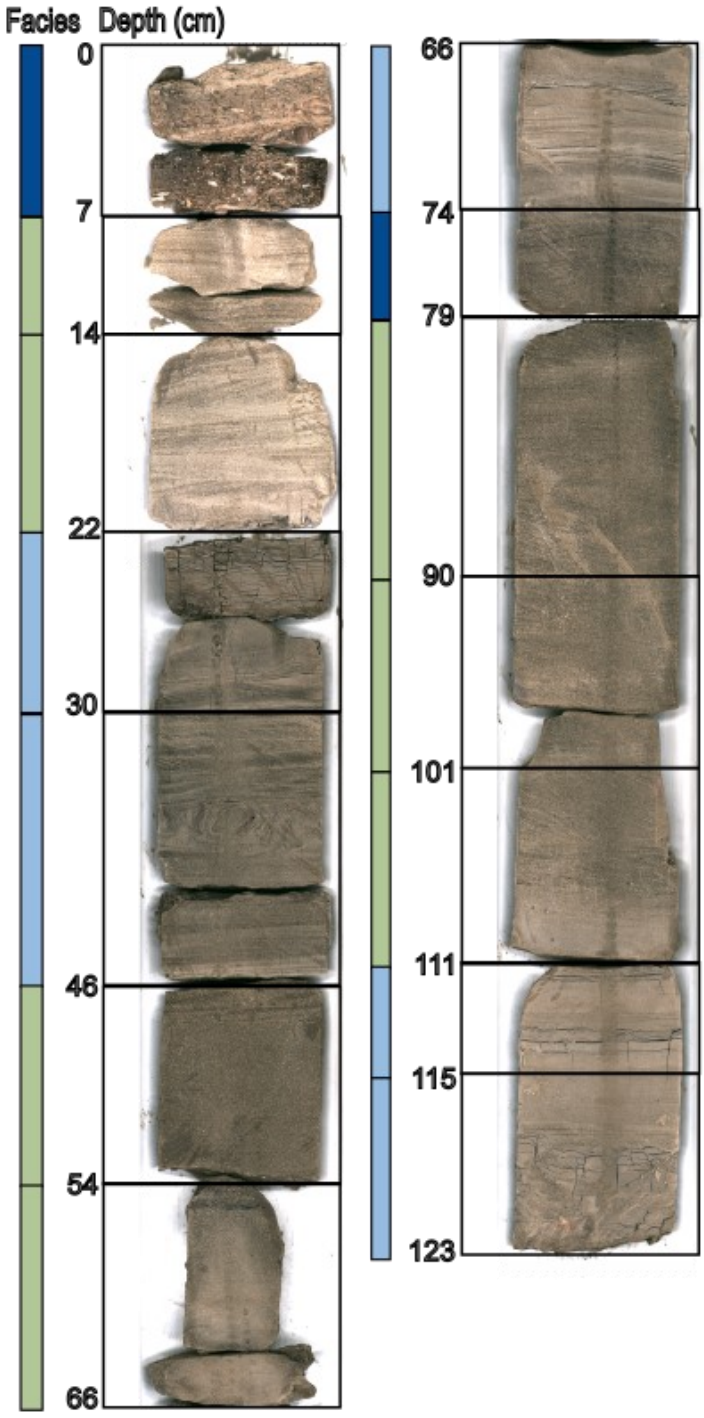

Figure A5. Ultra high-resolution images for alluvial core 2 (AC2). Facies A is represented by the dark blue, Facies B is represented by the light green, and Facies D is represented by the light blue.

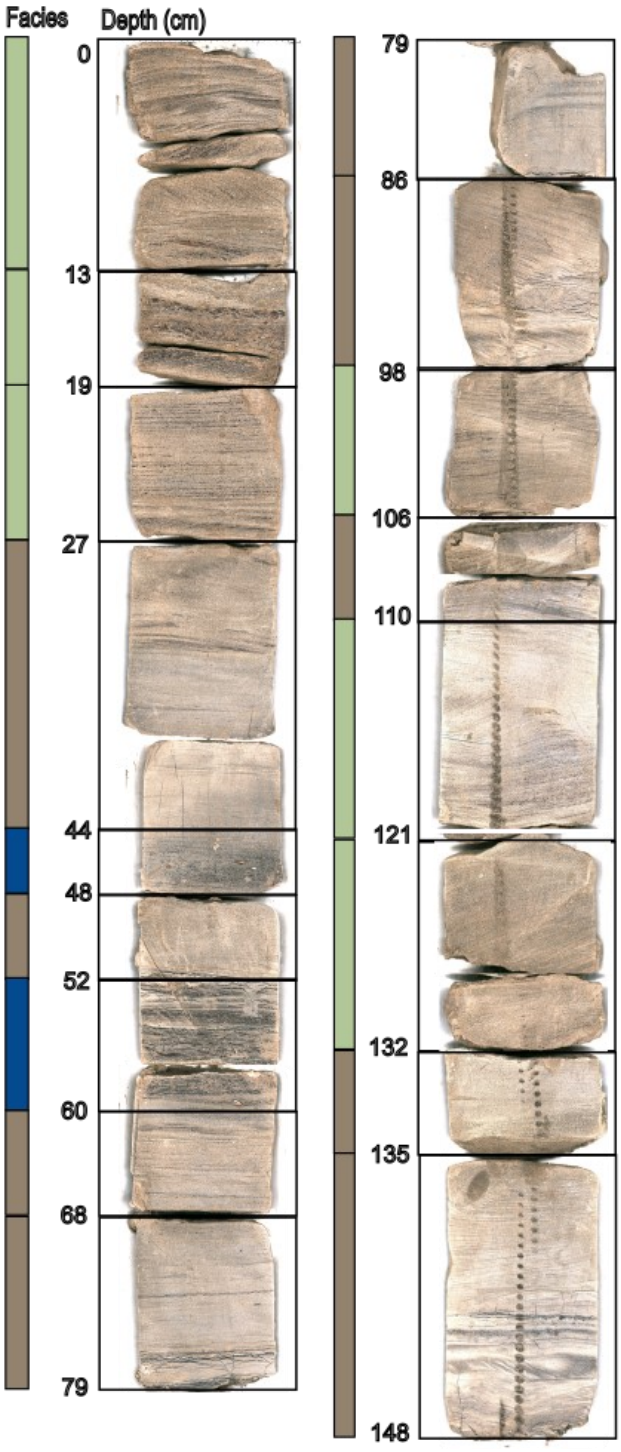

Figure A6. Ultra high-resolution images for alluvial core 3 (AC3). Facies A is represented by the dark blue, facies B is represented by the light green, and facies C is represented by the brown.

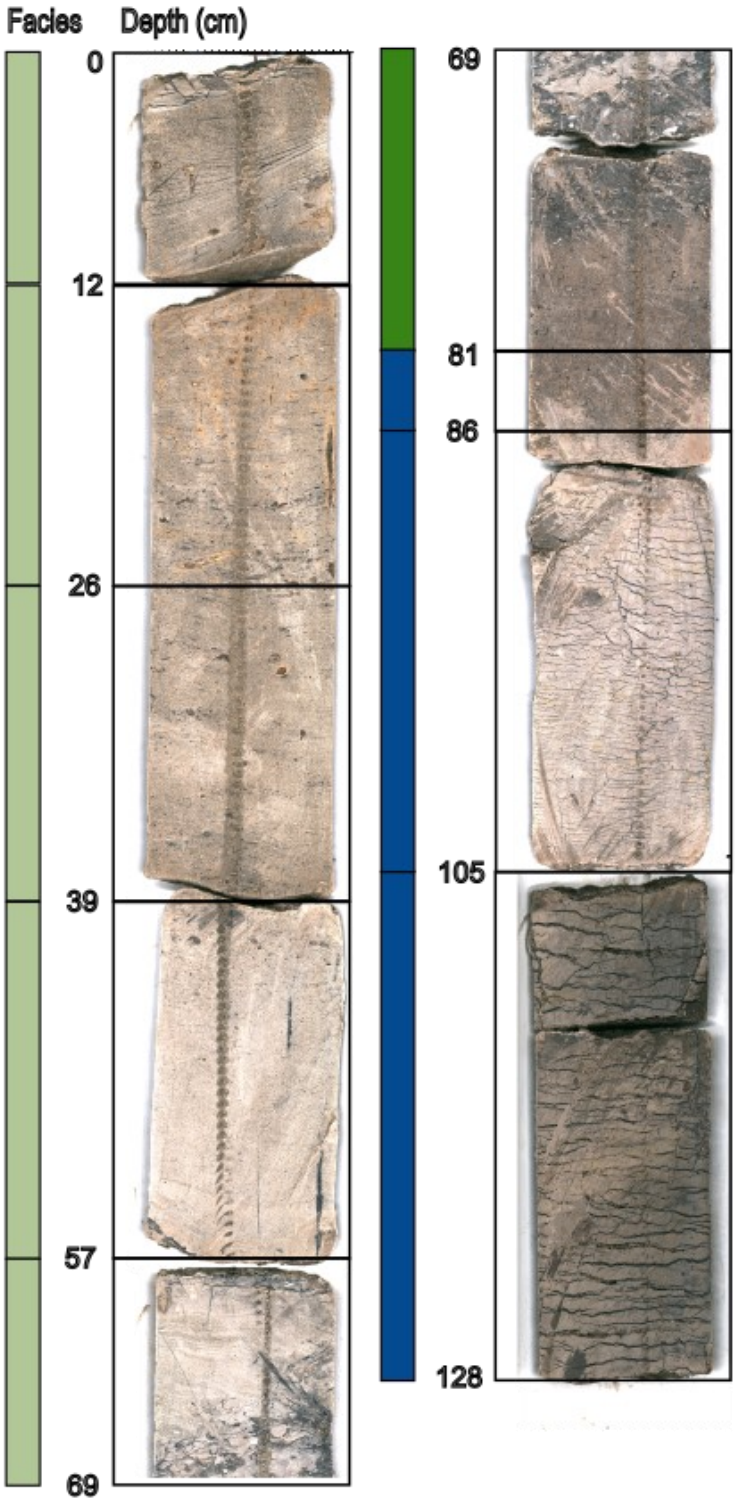

Figure A7. Ultra high-resolution images for terrestrial core 1 (TC1). Facies A is represented by the dark blue and Facies B is represented by the light green.

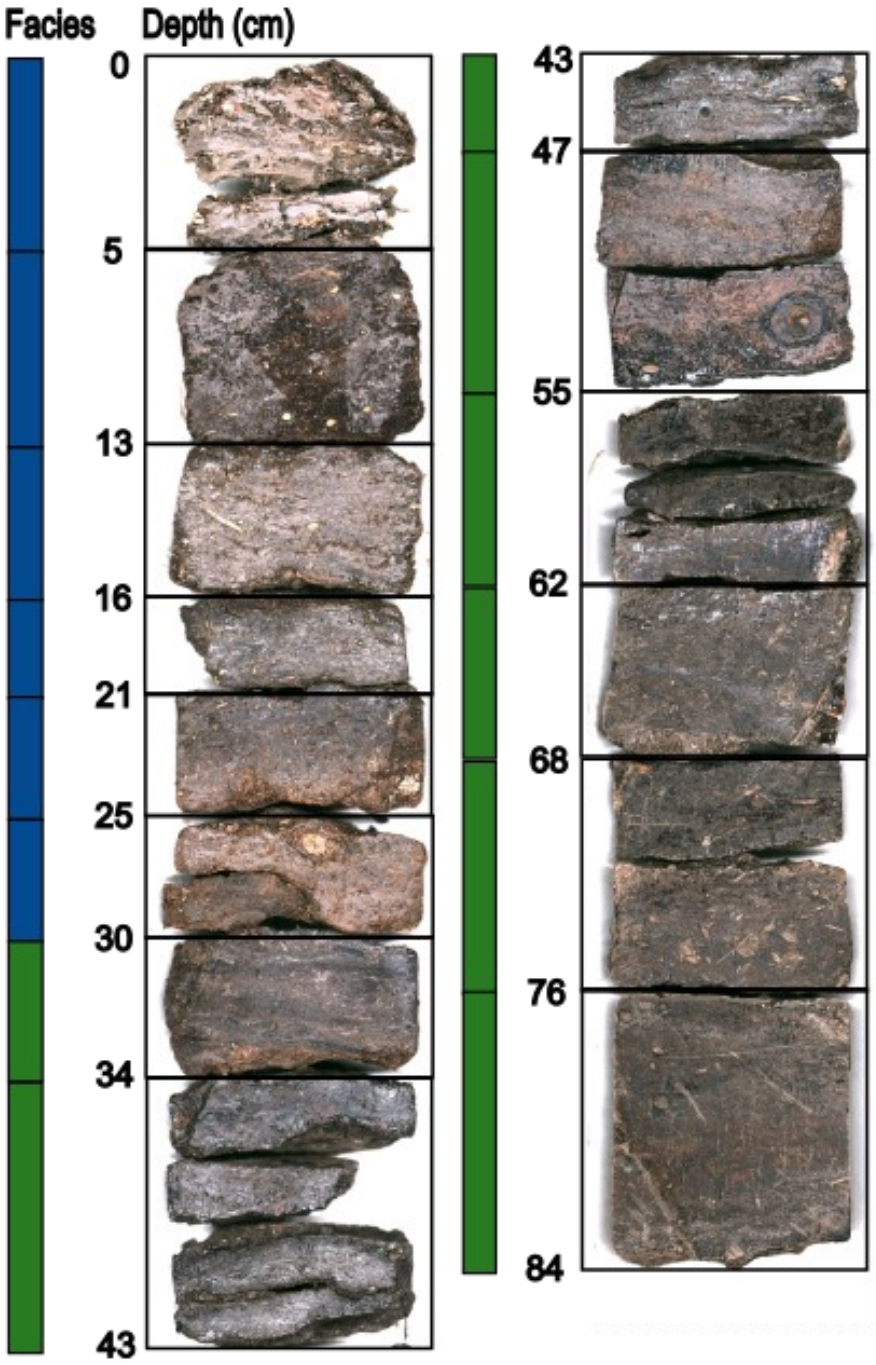

Figure A8. Ultra high-resolution images for terrestrial core 2 (TC2). Facies A is represented by the dark blue, and Facies F is represented by the dark green.

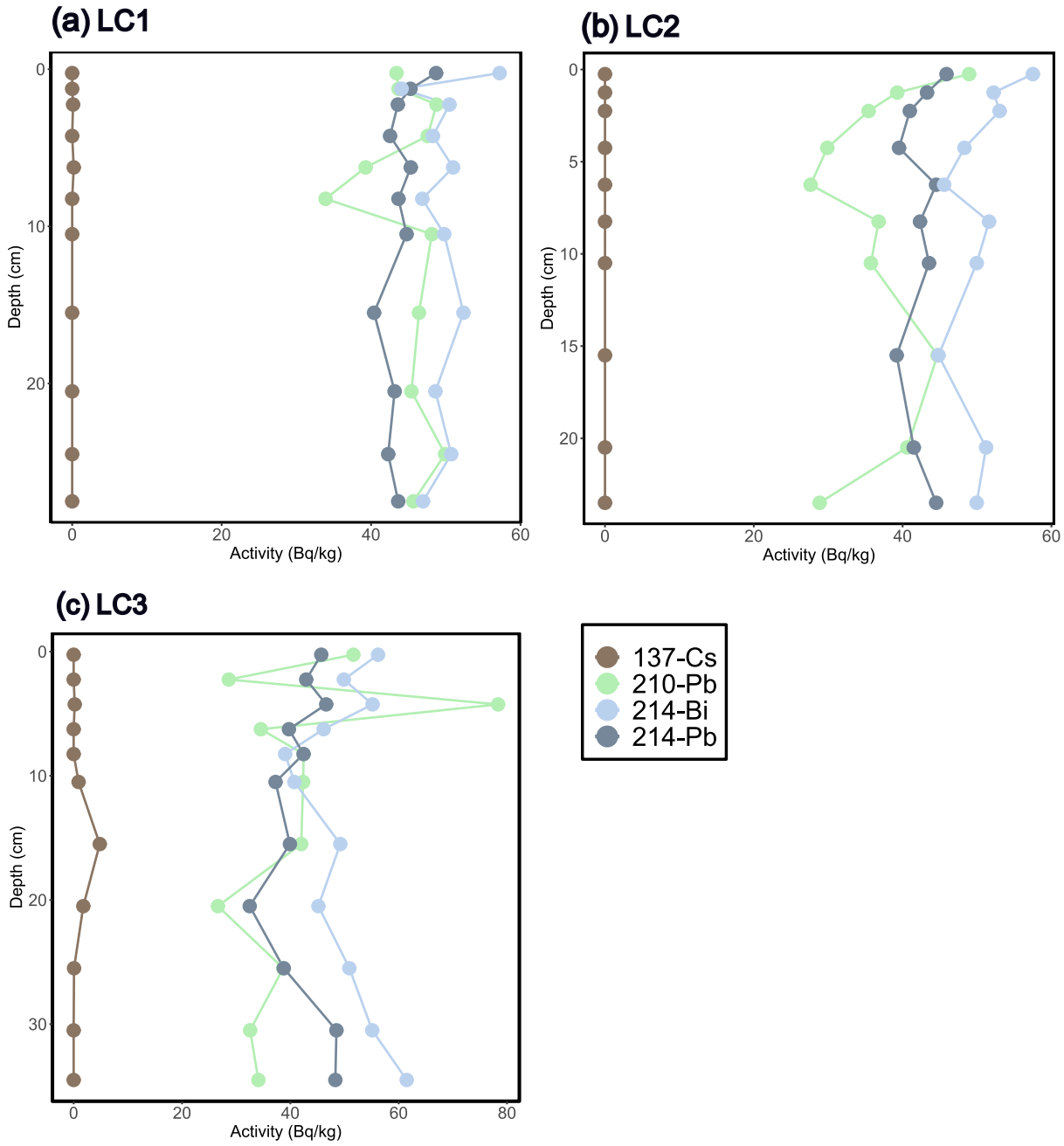

Figure A9. Activity for radioisotopes ^{214}Bi, ^{137}Cs, ^{210}Pb, and ^{214}Pb for lake cores LC1 (a), LC2 (b), and LC3 (c).

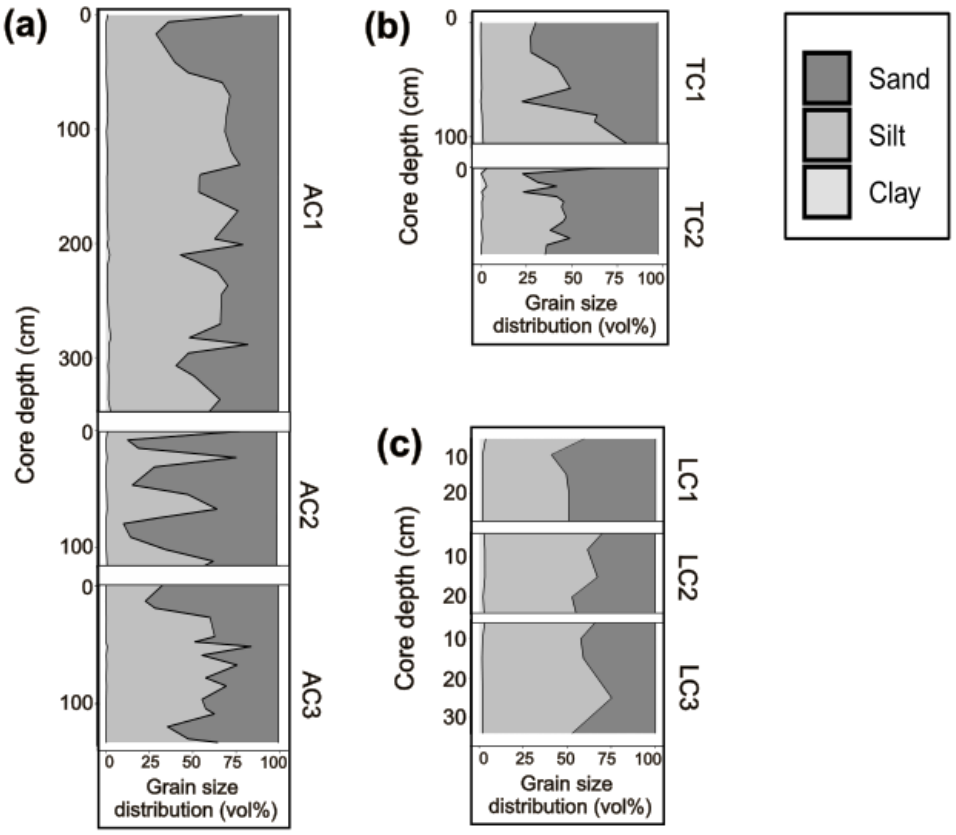

Figure A10. Grain size distribution by percent sand, silt, and clay for Willow Lake alluvial cores (a), forested overbank alluvial cores (b), and lake bottom cores (c).